FACULTY OF TECHNOLOGY

INFLUENCE OF CHROMIUM AND NIOBIUM CONTENT ON THE MECHANICAL PROPERTIES AND HEAT AFFECTED ZONE SIMULATIONS OF LOW-CARBON BAINITIC STEELS

Tun Tun Nyo

DEGREE PROGRAMME OF MECHANICAL ENGINEERING
Master's thesis
November 2019

ABSTRACT

Influence of chromium and niobium content on the mechanical properties and heat affected zone simulations of low-carbon bainitic steels

Tun Tun Nyo

University of Oulu, Materials and Mechanical Engineering

Master's thesis 2019, 65 p. + 3 Appendixes

Supervisors: Dr. Antti Kaijalainen and Jaakko Hannula

Controlled rolling followed by directing quenching results in steels with excellent mechanical properties, as well as saving cost by passing reheating cost after normalized rolling. The effect of six different combinations of niobium and chromium on microstructures and on mechanical properties of thermomechanically rolled and direct-quenched low carbon microalloyed steel plates were investigated. The target mechanical properties were 700 MPa yield strength with good impact toughness. Bainite was the dominant microstructure of all investigated steels. The prior austenite morphology and transformed microstructure was studied and compared to tensile properties, impact toughness, hardness and hardenability. Also, Gleeble simulation of heat affected zone (HAZ) was performed using $t_{8/5}$ of 5 s and 15 s to simulate weldability of steels. Four out of six compositions produced similar mechanical properties as S700 steel, which is currently produced in industry. 4 %Cr with 0.035% Nb can get better mechanical properties than with 0.06 % Nb. Addition of Cr also resulted in hardenability of austenite. Decrease of Cr content increased formation of quasi-polygonal ferrite, and therefore increased impact toughness and elongation and decreased the yield strength. Steels with 4% Cr were also observed to have negligible decrease in hardness at coarse grained heat affected zone (CGHAZ) compared to hardness level of base material.

Keywords: CGHAZ, direct quenching, inclusions, bainite, strength, impact toughness

TIIVISTELMÄ

Kromi- ja niobipitoisuuden vaikutus mekaanisiin ominaisuuksiin ja hitsaussimulointeihin matalahiilisessä bainiittiteräksessä

Tun Tun Nyo

Oulun yliopisto, Konetekniikan tutkinto-ohjelma

Diplomityö 2019, 65 s. + 3 liitettä

Työn ohjaajat: Dr. Antti Kaijalainen ja Jaakko Hannula

Kontrolloitu valssaus yhdessä suorakarkaisun kanssa mahdollistavat teräksille erinomaiset mekaaniset ominaisuudet sekä vähentävät kustannuksia, kun energiaa vievä normalisointivaihe voidaan jättää välistä. Työssä tutkittiin yhteensä kuuden erilaisella niobi- ja kromipitoisuudella olevan koostumuksen vaikutusta termomekaanisesti valssatun ja suorakarkaistun mikroseostetun matalahiilisen teräksen mikrorakenteeseen ja mekaanisiin ominaisuuksiin. Tavoitteena teräksen mekaanisille ominaisuuksille olivat 700 MPa myötölujuus sekä hyvä iskusitkeys. Bainiitti oli dominoiva mikrorakenne kyseisissä mikroseostetuissa teräksissä. Perinnäisen austeniitin morfologiaa ja siihen muodostunutta mikrorakennetta tutkittiin suhteessa mekaanisiin ominaisuuksiin, kuten lujuuteen, venymään, iskusitkeyteen ja karkenevuuteen. Lisäksi hitsattavuutta tutkittiin simuloimalla hitsauksessa syntyvää lämpovyöhykettä Gleeble-simulaattorilla kahdella eri $t_{8/5}$-ajalla; 5 sekuntia ja 15 sekuntia. Neljällä kuudesta tutkimuksesta koostumuksesta saatiin teollisesti tuotetun S700-teräksen kaltaisia tuloksia mekaanisten ominaisuuksien kannalta. Lisäämällä neljä prosenttia kromia ja 0.035% niobia saatiin parempia mekaanisia ominaisuuksia kuin lisämäällä pelkästään 0.06% niobia. Kromin lisäys myös paransi austeniitin karkenenevutta, kun taas kromin vähentäminen edesauttoi kvasipolygonaalinen ferriitin muodostumista ja siten kasvatti iskusitkeyttä ja venymää myötölujuuden kustannuksella. Lisäksi neljä prosenttia kromia sisältäneiden terästen karkearakeinen lämpövyöhyke pehmeni vähäisesti perusaineeseen verratuna.

Avainsanat: karkearakeinen lämpövyöhyke (CGHAZ), suorasammutus, bainiitti, sulkeumat, lujuus, iskusitkeys

ACKNOWLEDGEMENTS

I would like to express my gratitude to my supervisor Dr. Antti Kaijalainen for his comprehensive feedback and valuable guidance. I also want to thank Jaakko Hannula for giving me beneficial advice throughout this process. I would like to thank my family for their unending support and encouragement during these years. Furthermore, special thanks for the personnel at the Materials and Production Engineering and at SSAB's R&D department in Raahe and especially Tommi Liimatainen for contribution to my thesis. Finally, to all my colleagues/friends who gave me guidance and helped me to accomplish this thesis.

Oulu, 31/10/19

Tun Tun Nyo

TABLE OF CONTENTS

LISTS OF SYMBOLS AND ABBREVIATIONS

α	ferrite
γ	austenite
A_5	total elongation [%]
A_g	uniform elongation [%]
A_{r3}	austenite to ferrite transformation temperature on cooling [°C]
B_s	bainite start temperature [°C]
CB	coalesced bainite
CGHAZ	coarse grain heat affected zone
DQ	direct quenching
EBSD	electron backscatter diffraction
FESEM	field emission scanning electron microscope
FRT	finishing rolling temperature [°C]
GB	granular bainite
HV	Vickers hardness
J	joule
LB	lower bainite
M_f	martensite finish temperature [°C]
M_s	martensite start temperature [°C]
PAGS	prior austenite grain size
PF	polygonal ferrite
RD	rolling direction
R_m	tensile strength [MPa]
$R_{p0.2}$	yield strength [MPa]
t	plate thickness [mm]
T28J	28J transition temperature [°C]
TMCP	thermomechanical controlled processing
T_{NR}	non-recrystallisation temperature [°C]
UB	upper bainite

1 INTRODUCTION

Strength and toughness are two most important mechanical properties for the design of steel structures, pressure vessels, mobile cranes, booms or other similar components. Specific microalloying along with an optimized thermomechanical controlled processing (TMCP) has allowed high tensile properties to be achieved in combination with high levels of toughness.

In the last two decades there have been considerable advances in the theory and practice of accelerated cooling after controlled rolling. TMCP has become the most powerful and effective manufacturing process to improved strength, and superior low temperature toughness [1]. The microstructure, which is related with the mechanical properties of the hot rolled steels, is heavily influenced by the cooling process after hot rolling. The microstructure and mechanical properties of low carbon steel can be significantly improved by accelerated cooling process after hot deformation. Accelerated cooling result in bainite formation as well as, or instead of, ferrite formation.

Direct quenching can be considered a special case of thermomechanical processing, i.e. thermomechanical rolling integrated with direct quenching. With the conventional quenched and tempered process, the plates are typically hot rolled, air cooled after hot rolling, cut to required sizes, and then reheated to form austenite and finally water quenched to martensite or bainite and martensite mixtures. In the case of direct quenching, water quenching happens immediately after hot rolling from 1250 °C in which case austenite can be either recrystallized or non-recrystallized depending on the composition of the steel and the details of the rolling pass schedule prior to quenching. For instance, an increase in the total reduction in the non-recrystallization regime of austenite in conjunction with the reduced finish rolling temperature is an effective way to improve strength, toughness and ductility [2].

Steels with bainitic microstructures show the capacity to fulfil the requirements of high strength and low temperature toughness necessary for plate steels [3]. Niobium has been

added to low carbon steels to promote the formation of bainitic microstructures [4]. A fine grain microstructure is an optimum method for improving strength since unlike most other strengthening mechanisms, the improvement in strength is also accompanied by an improvement in toughness [5]. The use of niobium in low carbon bainitic steels is advantageous because when the amount of solute niobium is increased, retardation of austenite recrystallization is observed at significant higher temperatures, and because of its ability to promote the formation of bainite [6]. Addition of chromium is effective for improving the strength of low carbon bainite steel by increasing the amount of bainite transformation. Cr is not thought to be effective by solid solution strengthening and precipitation strengthening, but the main contribution of Cr is due to transformation strengthening [7]. Cr is an element that increases the strength of welds and their ability to hardened and is known as an element that promotes an increase in the proportion of bainite. Bainite has a desirable microstructure, increasing the toughness and strength of welds [8].

In this thesis, the TMCP and direct quenching process were employed to produce six different high-strength low-carbon bainitic steel with varying composition of niobium and chromium. And study the effects of the combined addition of niobium and chromium on the microstructure and mechanical properties in low-carbon micro-alloyed bainitic steels. The results are useful for designing low cost steel to compete in 700 MPa market. Heat affected zone simulation will be conducted at $t_{8/5}$ 5 s and 15 s to observe the softening effect via hardness measurement and Charpy impact test.

2 HOT ROLLING AND WELDING SIMULATIONS OF STEEL PLATES

2.1 Slab re-heating

To dissolve most of the carbide and nitride precipitates of microalloying elements before hot rolling at appropriate high temperatures to transform the as-casted microstructure to homogeneous fully austenitic microstructure, slabs are reheated [9]. The initial grain size and distribution of microalloying elements in the form of solid solution and precipitates are determined by the reheating temperature. Reheating temperature should be high enough and time should be long enough to be ensure that homogenous structure is obtained [10].

The temperature should be high enough so that all carbide and nitride precipitates are dissolved, and no pinning forces are remained, so that abnormal grain growth cannot occur. In abnormal grain growth, the structure consists of a few large grains and many small grains, which result in heterogeneous structure which prevent the steel from reaching desired mechanical properties. Sufficiently high reheat temperatures are selected so that abnormal growth stages surpassed, normal growth of the coarse grain structure is resumes [10].

2.2 Thermomechanical rolling and direct quenching

Thermomechanical controlled processing (TMCP) is a technique designed to improve the mechanical properties of materials by controlling the hot-deformation process in a rolling mill. This was originally designed to produce the required external shape of the product [11]. Controlled rolling, controlled-cooling and direct quenching are typical examples of thermomechanical controlled processing. Such processing saves energy in the manufacture of steel by minimizing or even eliminating the heat treatment after hot

deformation, thus increasing the productivity for high grade steels. It normally requires a change in alloy design and often reduces the productivity of the hot deformation process itself, but at the same time makes it possible to reduce the total amount of alloying additions and to improve weldability, whilst sometimes producing new and beneficial characteristics in the steel [12].

TMCP process has several advantages that can help overcome issues related to the addition of major alloying elements and conventional heat treatments. TMCP steels with added microalloys have been developed to manage the conflicting requirements of strength, toughness and weldability through grain refinement. TMCP effectively enables a reduction of the preheating temperature, thus lowering the rolling cost. As TMCP steels afford good weldability, they are highly valued in industries such as shipbuilding, offshore structures, pipelines and building construction [13].

TMCP is the sophisticated combination of well-defined deformation operations and well-defined heat treatment in a single production stage to control the microstructure of the steel being rolled. TMCP produces steels with the desired external qualities (dimensions, shape and surface quality) and acceptable mechanical properties. TMCP is normally considered as the final stage in the production of steels. By appropriate choice of deformation temperature and strain rate, the strength of steel can be increased. The strength of TMCP steel is higher than for normalized steel of the same composition. Thus, TMCP steel has a leaner composition (lower alloy content) than conventional normalized steel of the same strength [14].

TMCP consists of two stages in series namely (1) controlled rolling and (2) a subsequent accelerated cooling process as shown in Figure 1. During the rolling stage, the austenite grains are elongated into a pancake shape, which introduces crystallographic discontinuities such as ledges and deformation bands. These ledges and deformation bands remain until accelerated cooling starts when the rolling temperature is sufficiently low (less than 800 °C). The retaining deformation ledges and bands can act as potential heterogeneous nucleation sites for the austenite to ferrite transformations and contribute to grain refinement. TMCP achieves high strength by utilizing the transformation to

ferrite and bainite in addition to enhanced toughness, controlled rolling technology enhances toughness mainly by refinement of the ferrite microstructure [15].

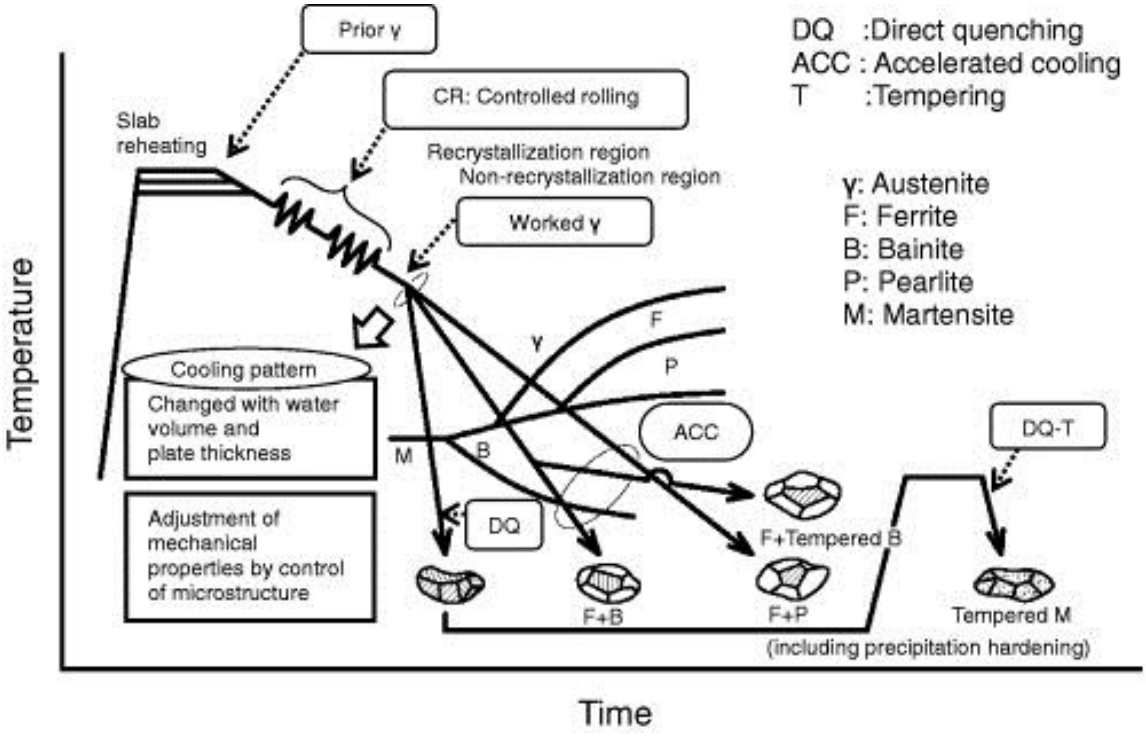

Figure 1. Concept of microstructure control by TMCP [16].

The most notable effect of TMCP is that steel with the same strength as conventional steels can be manufactured with a lower carbon equivalent (i.e. with lower alloy addition) through microstructural control. It has been demonstrated that the value of carbon required for TMCP steel to attain the same strength is 0.04 % to 0.08 % lower than that required for normalized steel. As a result, weldability (i.e. the preheating temperature required to prevent cold cracking at HAZ has been significantly improved in TMCP steels [17,18].

2.3 Weldability

Good toughness properties of a structural steel can be upset during welding procedures since toughness are very sensitive to microstructural change within heat-affected zone (HAZ). However, it is well-known that welding heat input will greatly affect the microstructure and mechanical properties in the heat affected zone (HAZ) of the steels. Especially, the heat input will increase grain growth in the region near the fusion line, called the coarse gain heat affected zone (CGHAZ). The weld coarse grained HAZ (CGHAZ) next to the fusion line having the lowest toughness among the various regions within a HAZ because of coarse grain structure. The grain growth leads to a decrease in toughness of the welded joints [19]. Therefore, the advantage of the steels cannot be fully exerted. In the present work, CGHAZ using Gleeble 3800 thermomechanical simulator (Figure 2) was investigated.

The weldability of steels is influenced primarily by the carbon content. At higher carbon levels, steels may need either pre- or post- weld heat treatment in order to prevent stress build up and weld cracking. If the Carbon Equivalent (CE) is 0.4 or below, no pre- or post- weld thermal treatment is needed. It has been found that preheating was beneficial between 0.35 and 0.55 CE. Above 0.55 CE, usually both pre- and post- weld heating has been used to relieve stress and prevent cracking [20].

Figure 2. Gleeble 3800 thermomechanical simulator

3 MICROSTRUCTURES OF LOW CARBON STEELS

3.1 Bainite

Bainitic microstructures in steels can offer attractive combinations of strength and toughness, and therefore those steels are now being increasingly used to produce the levels of strength increasingly demanded by end users. The bainitic microstructure derives its favorable balance of strength and toughness from the mixture of ultrafine ferrite crystals with second phases distributed between or inside ferrite. There are financial benefits to be realized by developing bainitic steel products with desired properties without the need for subsequent heat treatment.

3.1.1 Isothermally formed bainite

The morphological characteristics of isothermally formed bainite are divided into two types, upper bainite and lower bainite according to the microstructural characteristics of carbides. In case of conventional steels, the upper bainite formed at higher temperatures consists of fine ferrite plates each of which is about 0.2 μm thick and about 10 μm long. The plates grow in clusters called sheaves. Within each sheaf the plates are parallel and of identical crystallographic orientation each with a well-defined crystallographic habit. The individual plates in a sheaf are often called the subunits of bainite. They are separated by low misorientation boundaries or cementite particles. The major microstructural constituent is either needle or laths of ferrite. Carbides, mainly Fe_3C, grow at the interface of the ferrite plates [21].

Typically, upper bainite (UB) consists of elongated laths ordered in packets with cementite particles distributed over the lath boundaries. Individual bainite laths are typically oriented at a 40–60° angle to the rolling direction. In the presence of microalloying elements, bainitic ferrite laths may contain a fine dispersion of precipitation-strengthening (microalloy) carbides [22].

Lower bainite is the predominant morphology in cast irons and in steels. It has a microstructure and crystallographic features, which are like those of upper bainite. The major distinction is that the transformation is at lower temperature so that carbides can also precipitate inside the plates of ferrite. There are, therefore, two types of carbides: those which may grow from the carbon enriched austenite, and others which precipitate inside the supersaturated bainitic ferrite [21].

The difference between upper and lower bainite is also based on whether the transformation temperature is above or below approximately 350 °C, although it has been shown that the distinction is not universally applicable. Upper bainite comprises a lathlike morphology, and the austenite/ferrite habit plane is thought to be near {111}γ/{110}α. Lower bainite is generally reported to have a plate-like morphology in isothermally transformed steels, with an irrational habit plane somewhat further away from{111}γ. The carbide in lower bainite generally consists of a single crystallographic variant inclined to the apparent longitudinal axis of ferrite, although multiple variants have also been reported [21].

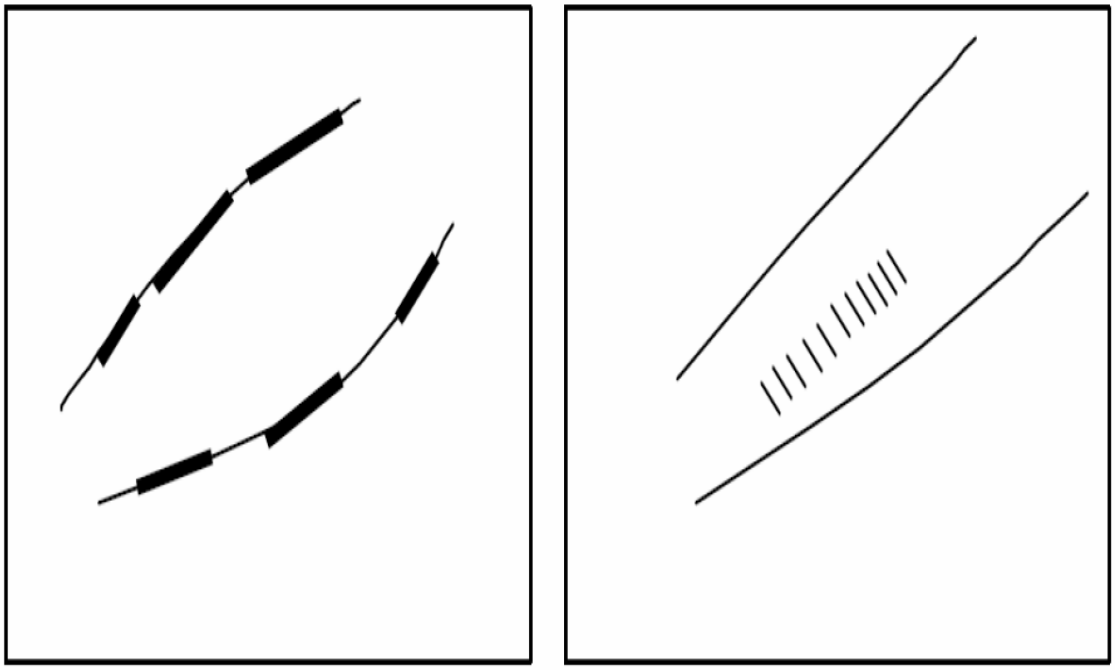

Figure 3. Two carbide shapes in bainite: left: upper bainite, right: lower bainite [22].

3.1.2 Continuously cooled bainite

Granular bainitic microstructure is usually used to describe the bainite that occurs during continuous cooling transformation. This terminology is used widely in industry, where most steels undergo non-isothermal heat treatments. Granular bainite cannot readily be distinguished from ordinary bainite when examined using transmission electron microscopy, because its mechanism of formation is not different. However, because the microstructure forms gradually during cooling, the sheaves of bainite can be rather coarse. The optical microstructure then gives the appearance of blocks of bainite and austenite, so that it is appropriate to use the adjective 'granular'. In typical, granular bainite does not contain carbides in the microstructure. The final microstructure consists of both retained austenite and some high-carbon martensite in addition to the bainitic ferrite, due to carbon being partitioned from bainitic ferrite which in turn stabilized the residual austenite [24].

This mixed microstructure has got potential advantages such as:

- Cementite is responsible for initiating fracture in high-strength steels. Its absence is expected to make the microstructure more resistant to cleavage failure and void formation.

- The bainitic ferrite is almost free of carbon, which substantially strengthens the ferrite.

- The microstructure derives its strength from the fine grain size of the ferrite plates.

- The ductile films of austenite, which are intimately dispersed between the plates of ferrite, have a crack blunting effect. They further improve the toughness by increasing the work of fracture as the austenite is induced to transform to martensite under the influence of the stress field of a propagating crack.

- Steels with bainitic ferrite and austenite microstructure can be obtained without the use of expensive alloying elements.

However, to realize these beneficial effects, both the ferrite and austenite need to be in a fine-grained structure [25]. This grain refinement could be achieved by the prior compressive deformation of austenite, which promotes the formation of granular structure, reduces the length of bainitic laths and by the alloying additions of inexpensive alloying elements [26].

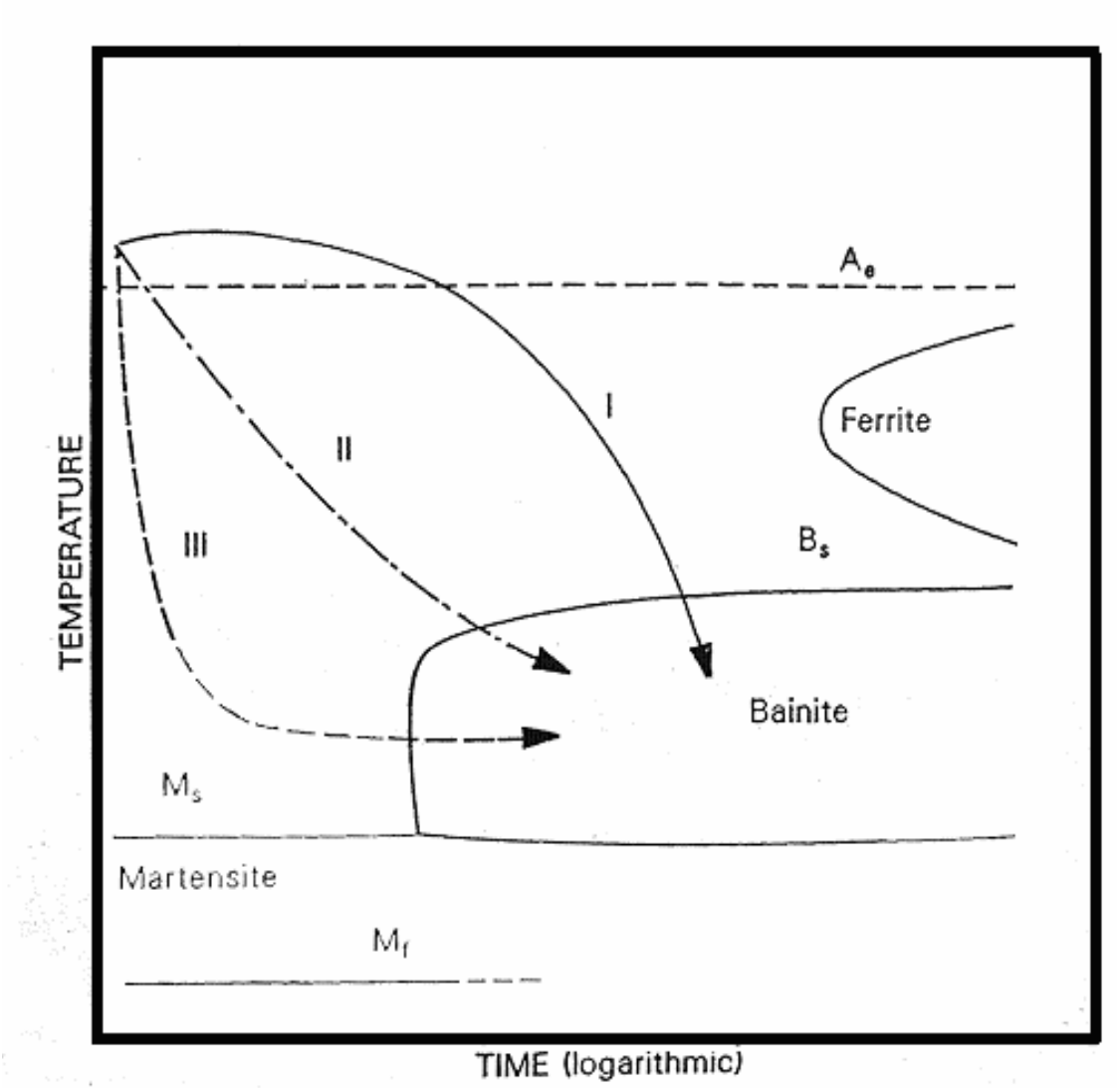

Figure 4. Schematic representation of a CT diagram showing formation of granular bainite (path I), upper bainite (path II), and lower bainite (path III) [26].

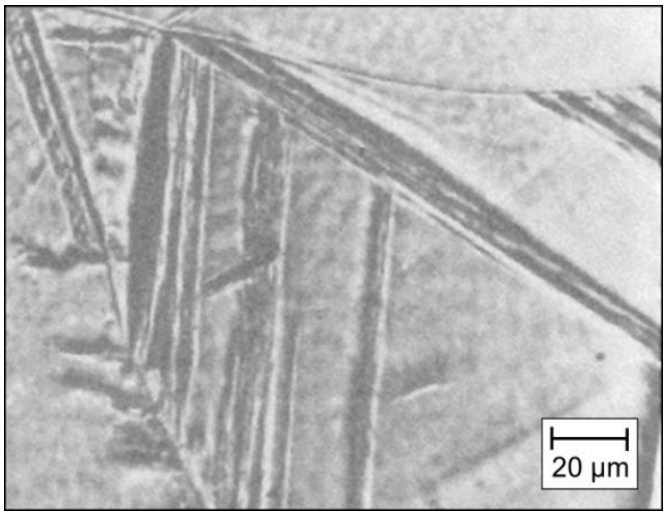

(a)

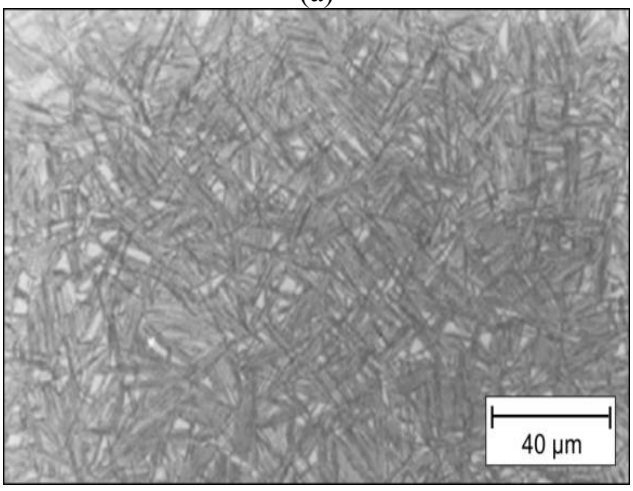

(b)

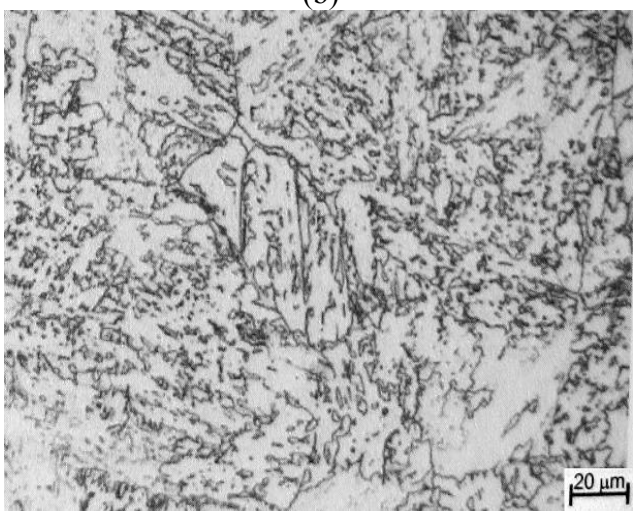

(c)

Figure 5. Example of (a) upper bainite, (b) lower bainite and (c) granular bainite microstructure [24].

A general characterization of bainitic microstructures has been performed using optical and scanning electron microscopy. More detailed microstructural information, at the scale on which the properties of bainitic microstructures are controlled were obtained using high resolution field scanning electron metallography. Clear differences were noted between upper, lower and granular bainite. Lower bainite has a high proportion of boundaries with misorientations in the range 50-60° and very few boundaries with low misorientations (<20°). Upper bainitic structures has a high proportion of low-angle boundaries with low misorientations (<20°) and fewer high-angle boundaries with misorientations (>50°). In the granular bainite (with irregular ferrite) the distribution of grain is more random with abroad peak at about 45° [22].

3.2 Ferrite

3.2.1 Polygonal or equiaxed ferrite

The ferritic microstructure which forms at the highest temperatures and slowest cooling rates in low-carbon steels is nucleated as grain-boundary allotriomorphs and grows into equiaxed grains. In view of the equiaxed grain geometry, this type of ferrite is referred to as equiaxed or polygonal ferrite (PF). Polygonal ferrite is readily identified in the light microscope and is characterized by very low dislocation densities and the absence of substructure, as revealed by the transmission electron microscope. Figure 6a shows an example of polygonal ferrite. Due to impingement, there is considerable grain-boundary curvature in the isothermally formed ferrite in Figure 6a, but the ferrite grain boundaries are smooth and continuous on the scale of the light microscope. Nucleation of equiaxed ferrite starts at austenite grain corners. Thus, the ferrite interfaces cross original austenite grain boundaries, and the parent austenite grain structure is rendered indistinguishable in specimens largely transformed to polygonal ferrite. [27]

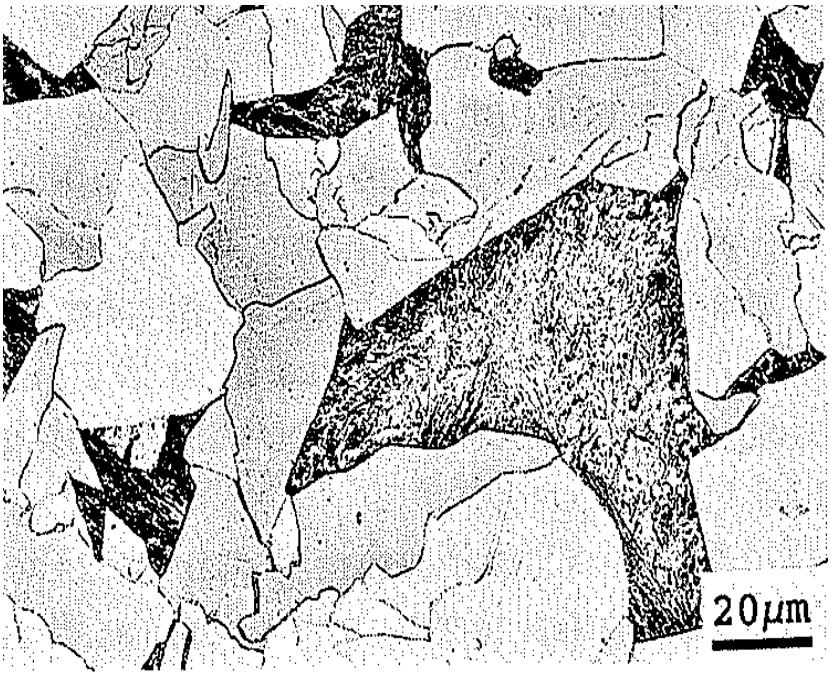

(a)

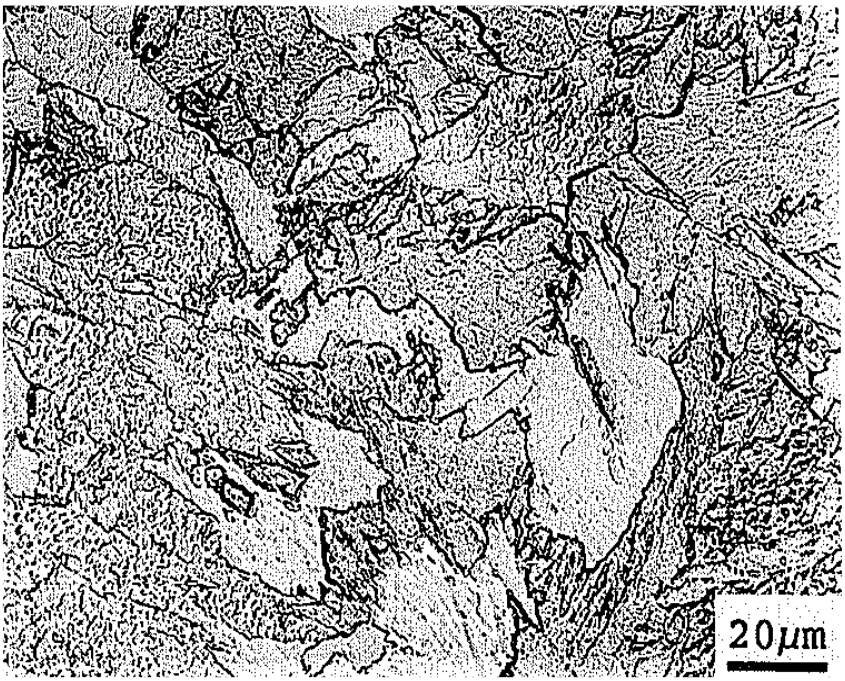

(b)

Figure 6. (a) Polygonal ferrite (light grains) and (b) quasi-polygonal ferrite [27].

3.2.2 Quasi-polygonal ferrite

In very low carbon steels and irons, it is possible by rapid cooling to go from single-phase austenite to single phase ferrite without a composition change. Cooling, however, must be rapid enough to minimize partitioning in the intervening two-phase ferrite-austenite field. Under these conditions, the microstructure formed consists of relatively coarse ferrite grains, and therefore, is referred to as quasi-polygonal ferrite. The ferrite grains, however, have irregular grain boundaries and often show etching evidence of substructure. Figure 6b shows an example of quasi-polygonal ferrite. [27]

Practical interest is now expressed because continuously cooled low-carbon steels with quasi-polygonal ferrite microstructures show the potential of excellent combinations of strength and ductility [28]. At the migrating boundaries, interstitial or substitutional atom partitioning may occur, causing massive ferrite grains with irregular and the sharp boundaries. In contrast to polygonal ferrite, massive ferrite, as shown by transmission electron microscopy, contains a high dislocation density, dislocation sub boundaries and apparently even M/A constituent [27].

4 ALLOYING ELEMENTS AND INCLUSIONS

An iron alloy containing carbon are called steel. In bainitic steel, microalloying with elements such as Nb, Ti, V, and B results in strengthening as well as grain refinement. Elements are added in small quantities, usually below 0.1 wt.%, and that is why these are called microalloyed elements. Phase transformation temperatures can be inhibited by adding substitutional alloying elements, such as Mo, Ni, Cr and Cu, which also results in strengthening, since phase transformation temperature has strong effect on the strength of bainitic structures. When designing the low carbon steels with bainitic structures, carbon level should be low or ultralow. Required transformation temperature is achieved by alloying combination with TMCP [29].

4.1 Niobium

Niobium is used to suppress recrystallization between passes during hot rolling. Such suppression can either be done by solute drag, in the case of Nb present in solid solution, or by strain-induced transformation in which niobium carbides/nitrides precipitate and pin austenite grain boundaries [30]. The latter mechanism is usually preferable, since pancaked austenite provides a large number of nucleation sites for the austenite to ferrite transformation [31].

During thermomechanical rolling, the strain induced precipitation of microalloying elements such as Nb plays an important part in controlling the microstructure. Nb delays the onset of austenite recrystallization [3]. Because of the non-recrystallized nature of austenite, there is a plentiful supply of heterogeneous ferrite nucleation sites (ledges and deformation bands) for the subsequent cooling process. Nb also induces other effects such as during the austenite to ferrite transformation upon cooling it precipitates in the ferrite matrix and enhances its strength via the precipitation strengthening mechanism [3]. The crystal structure of the precipitates does not fit well in the ferrite lattice and this incoherency between the ferrite and precipitates results in increased strength.

In solid solution, niobium has also a strong effect in lowering the γ/α transformation temperature among commonly used microalloying elements, and at higher cooling rate, this effect is clearly observed (Figure 7). By lowering the transformation temperature of thermomechanically rolled plates with accelerated cooling, the grain size of polygonal ferrite is refined and the volume fraction of bainite is increased. [33]

Niobium is also expected to affect the TTT curve depending on the state of Nb. As a strong carbide former, Nb can decrease the hardenability of steel by removing carbon from the austenite [33]. In this situation the precipitates of Nb (NbC or Nb_2C) refine the grain structure, improving strength and toughness; however, hardenability decreases as previously explained. If present in solid solution in the austenite phase, Nb lowers the austenite to ferrite transformation temperature and increases the hardenability of the austenite [33].

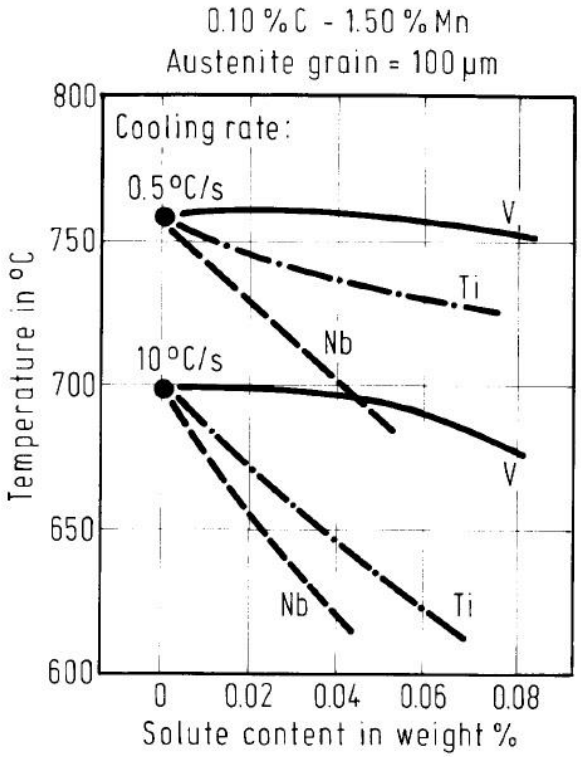

Figure 7. Ar_3 temperatures of microalloyed steels with equal austenite grain size [32].

4.2 Chromium

Cr is not a strong hardenability agent as compared to some other elements such as manganese (Mn) or molybdenum (Mo). However, it is very cost effective (degree of hardenability increase/relative cost of alloying element). Cr has also a strong tendency to form hard and stable carbides. The presence of Cr carbide also gives structural steels the ability to resist softening at higher temperatures. However, it also means that for a given hardness level, Cr steels need higher tempering temperatures, or longer tempering times, than the plain C steels. This effect increases with increasing Cr content of the steel. The presence of Cr carbide also gives structural steels the ability to resist softening at higher temperatures. This leads to greater creep and stress rupture resistance [34].

Chromium is an element that increases the strength of welds and their ability to harden and promotes an increase in the proportion of bainite. Since bainite improves the toughness and strength of a weldment, as it becomes finer, it acts as an obstacle for cleavage fracture. In the grain size distribution using EBSD, a specimen with higher Cr content showed a higher micro-grain distribution. Therefore, when the Cr content increased, a higher absorbed energy was measured in the impact test results. Since the toughness and yield strength are inversely proportional, the value of yield strength obtained from the tensile test is low for a specimen in which a high fraction of acicular ferrite was formed because a large amount of Cr was added. In addition, because Cr is a ferrite-stabilizing element, the measured hardness value of a specimen with higher ferrite content was higher. Cr increases the hardenability of steel while there is a minimal effect on the ductility.[4]

4.3 Role of inclusions

Inclusions occur typically in low or very low volume fractions but play an important role in many properties of steel. Inclusions play a decisive role in processes involving ductile fracture, fatigue and corrosion, for instance. These are some of the properties more

relevant to the performance of steel in structural and mechanical applications. Furthermore, Inclusions may influence nucleation during phase transformations of steel.

Many commercially available elements that are acceptable in steel composition have a high affinity for oxygen and canthus be used as deoxidizers, forming non-metallic deoxidation products when added to the liquid steel [36]. Examples are silicon, manganese and aluminum. Deoxidation products can become important oxide inclusions. In the case of sulfur, on the other hand, only elements with low solubility in iron (such as Ca and Mg) or rare earths, have sufficiently high affinity for sulfur to form sulfides at the liquid metal temperatures [35]. Thus, most of the sulfur in steel must be removed from solution by slag refining and the rest, by precipitation reactions occurring mostly during solidification. The most common sulfide precipitating during solidification is MnS.

Some properties of inclusions have a key importance on how they influence the behavior of steels. These include plasticity or hardness as a function of temperature. Inclusions that are plastic at the working temperature will deform when steel is worked. This will result in elongation of the inclusions along the major working directions. This introduces, in many cases, shape anisotropy in the inclusions. This results in anisotropy of the properties influenced by inclusions [36].

Ductile fracture processes are important in structural and mechanical applications of steel. They influence ductility, formability and toughness. Ductile fracture of steels generally occurs by the nucleation, growth and coalescence of microvoids. These voids nucleate by debonding or cracking of Inclusions and second phase particles [37]. The process is in most cases dominated by the nucleation and growth of microvoids preferentially around Inclusions and their coalescence by necking of the metal between inclusions. Hence, there is a significant effect on properties related to ductile fracture [38].

Crack origination and propagation in fatigue one must consider size and volume fraction of Inclusions. Crack origination may occur “in the matrix” or related to second-phase

particles. It seems that for lower strength steels, a critical crack size larger than the larger Inclusions is needed for fatigue to occur [39].

5 EXPERIMENTAL PROCEDURES

5.1 Investigated compositions

The six casts for this thesis have been manufactured by Outokumpu, Tornio. The compositions and carbon equivalent by using Equation 1 of each steel are shown in Table 1.

$$CEV\ (\%) = C + Mn/6 + Cr/10 + Ni/20 + Mo/50 + V/10 + Cu/40 \text{ [20]} \quad (1)$$

The casts were produced and studied in two stages .In first stage, the effect of Cr content in the range of 1-4 wt.% on the microstructure and mechanical properties of controlled hot-rolled and direct-quenched steel plates containing of 0.06 wt.% Nb has been studied to evaluate the effect of chromium on hardenability of these steels, and to produce the sufficient strength level. In second stage, additional three casts with variating of Cr and Nb content were produced to form final DOE matrix (Figure 8).

Table 1. Chemical compositions and impurity levels of investigated steels (in wt.%). The oxygen and nitrogen levels are based on combustion analysis, while other were analysed by an optical emission spectrometer. Equation 1 was used to determinate the carbon equivalent (CEV).

Stage 1	**C**	**Nb**	**Cr**	**Si**	**Mn**	**S**	**Al**	**O**	**N**	**CEV**
	%	**%**	**%**	**%**	**%**	**%**	**%**	**%**	**%**	**%**
0.06Nb4Cr	0.036	0.064	4.00	0.154	0.917	0.0030	0.044	0.0025	0.0061	0.58
0.06Nb2.5Cr	0.041	0.066	2.5	0.168	0.945	0.0031	0.052	0.0027	0.0062	0.44
0.06Nb1Cr	0.041	0.065	1.0	0.211	1.02	0.0034	0.050	0.0021	0.0059	0.30
Stage 2	**C**	**Nb**	**Cr**	**Si**	**Mn**	**S**	**Al**	**O**	**N**	**CEV**
	%	**%**	**%**	**%**	**%**	**%**	**%**	**%**	**%**	**%**
0Nb2.5Cr	0.042	0.002	2.5	0.181	1.06	0.0030	0.050	0.0021	0.0058	0.47
0Nb4Cr	0.041	0.002	4.0	0.211	1.07	0.0028	0.051	0.0020	0.0060	0.62
0.035Nb3.3Cr	0.040	0.032	3.25	0.213	1.06	0.0029	0.049	0.0021	0.0056	0.54

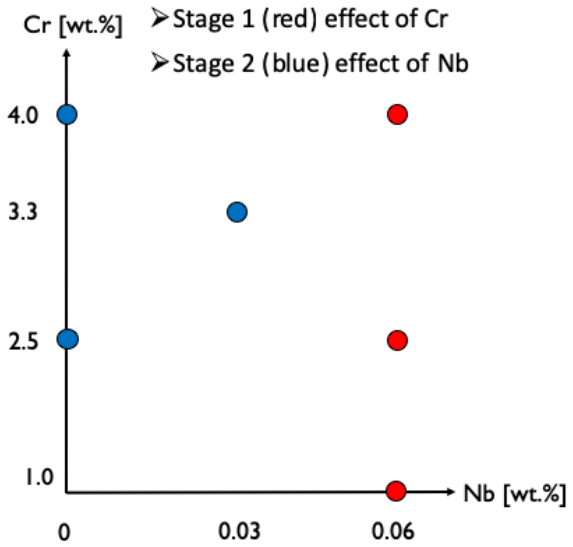

Figure 8. DOE matrix of the investigated compositions.

5.2 Austenite grain growth study during slab reheating

The effect of compositions on the austenite grain growth behavior was studied. The slabs are soaked sufficient time to ensure homogeneous structure and temperature. In this study, four different target soaking temperatures were used: 1100, 1150, 1200 and 1250 °C. The heating rate used in this experiment was based on thermocouple measurements from approximately 60 mm thick steel slab, which was heated up to 1250 °C before hot rolling in our laboratory scale rolling mill. Samples (~15x15x10 mm^3) were used for studying austenite grain growth. To reach the peak temperature, total time was approximately 120 minutes. Hold at peak temperature was about 10 minutes before water quenched. Laser scanning confocal microscope was used to take images of samples for grain size calculation

5.3 Controlled hot rolling and direct quenching of the plate

The controlled rolling process was carried out on a 1000 kN laboratory mill, with 250 mm diameter rolls (Figure 9). A 60 mm thick steel slab was placed into a furnace which has been preheated to 1250 °C and socked for two hours, and then it was rolled into 12 mm thick plate in 6 passes. The finishing rolling temperature was about 880 °C. The pass schedule can be seen in Figure 10. After hot rolling, direct quenching in a water tank was used to achieve a high cooling rate (~40-50 °C/s).

Figure 9. Laboratory scale rolling mill.

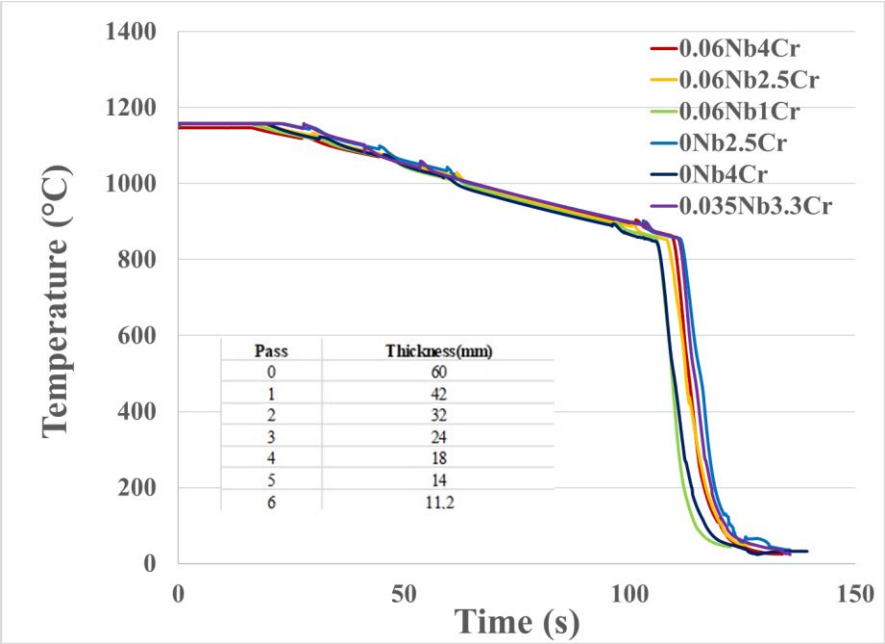

Figure 10. Cooling curves and pass schedule of studied steels.

5.4 Sample preparation

The samples for the mechanical testing and microstructure characterization were taken from the laboratory hot-rolled plate as shown schematically in Figure 11.

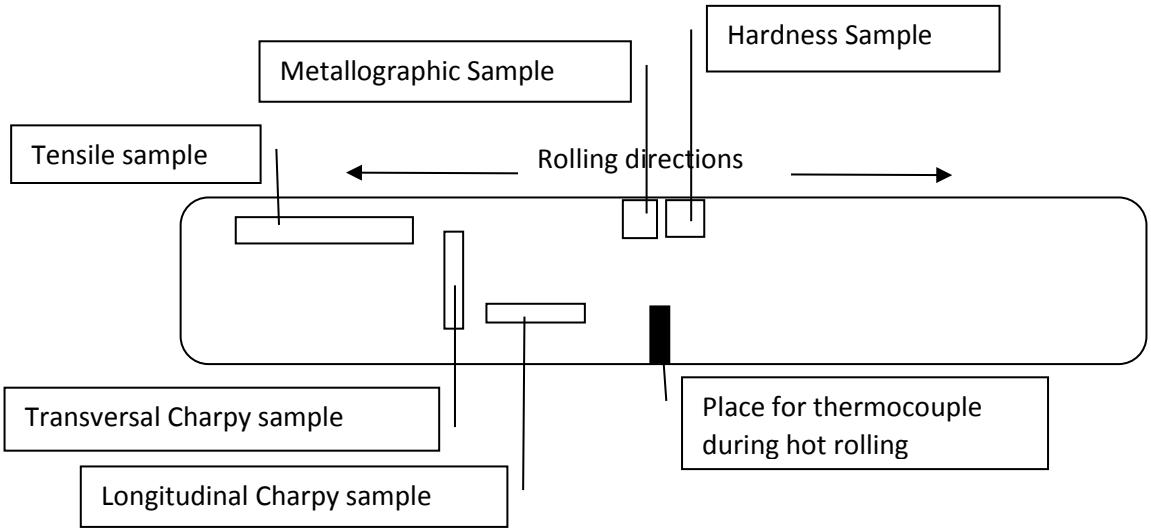

Figure 11. Schematic presentation of where the samples are taken from rolled plate and which direction compared to rolling direction.

5.5 Mechanical testing

5.5.1 Tensile test

The tensile test is one of the most commonly used tests for evaluating materials. The test involves straining a specimen in tension, generally to fracture, for determining mechanical properties such as, tensile strength, yield strength, elongation and reduction of area. Longitudinal tensile flat specimens with thickness of approximately 11.7 mm, width of 20 mm and a parallel length of 120 mm were tested at room temperature using MTS 810 testing machine fitted with a 100 kN load cell and measurements are based on SFS.EN 10002.1 standard. Three tests are carried out for each steel.

5.5.2 Impact test

The Charpy impact test gives an indication of the amount of energy absorbed by the material at fracture (the impact toughness). Transversal and longitudinal impact toughness was measured on normalized Charpy V-notched (10 mm x 10 mm x 55 mm) samples at temperatures between −120 °C and 20 °C using a 300 J Charpy testing machine. Impact toughness tests were made by machine called D6800-Mannheim. Specimens were tested in accordance with the steel standard BS EN 10 045.1: 1990 [40]. Three specimens were tested at each temperature for every alloy.

5.5.3 Hardness test

The Vickers hardness test method consists of indenting the test material with diamond indenter, in the form of a right pyramid with square base and an angle of 136 degrees between opposite faces subjected to a load of 1 to 120 kg. Hardness tests were done by using a DURAMIN A-300 testing machine with 10kg indenter load (HV10). A representative hardness value was obtained from the mean of 5 sets of seven suitably spaced hardness impressions at the intervals of 1.5 mm. The hardness measurements were performed on as-polished samples. The location of hardness measurements is shown in Figure 12. The spacing between each indentation was at least three times the diagonal length to ensure that each measurement was independent of any others.

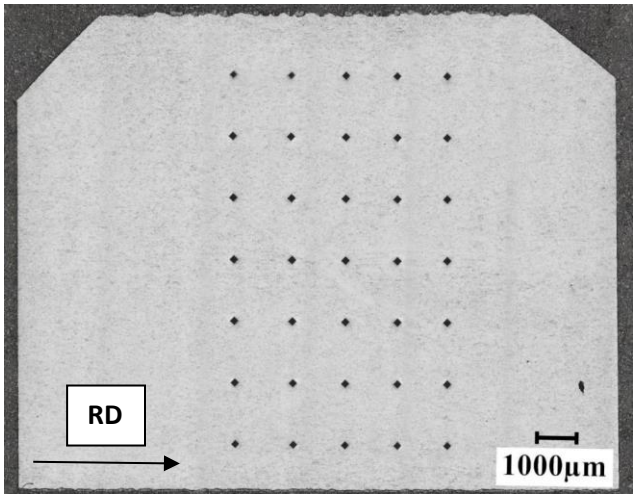

Figure 12. Location of hardness measurements.

5.6 Microstructure characterizations

Characterization of microstructures was carried out by using light optical microscopy (LOM) and field emission scanning electron microscopy (FESEM).

5.6.1 Light optical microscope (LOM)

Specimens, longitudinal to the hot rolling direction, were mounted and mechanically ground and polished with 3 μm and 1 μm diamond paste for metallographic examination. A 2 % Nital etching solution was used reveal general microstructure and with saturated picric acid and wetting agent plus a few drops of Hydrochloric acid to reveal prior austenite grain boundaries and observed with Nikon Eclipse MA100 light optical microscope.

5.6.2 Field emission scanning electron microscope and electron backscatter diffraction (FESEM-EBSD)

Specimens, longitudinal to the hot rolling direction, were mounted and mechanically ground using silicon carbide abrasive paper down to mesh number 1200 before polished with 3 μm and 1 μm diamond paste for metallographic examination. A 2 % Nital etching solution was used reveal microstructure to be observed under field emission scanning electron microscope (FESEM). FESEM images are taken using ZEISS SIGMA at the quarter and center plate thickness positions.

Electron backscatter diffraction (EBSD) samples were polished with 0.04 μm silica as final step for EBSD analyses. EBSD analyses revealed the effective grain and lath sizes of the microstructures together with grain boundary misorientation distributions. EBSD acquisitions were made using an accelerating voltage of 15 kV, working distance of 15 mm and a step size of 0.2 μm.

On each sample, two separate regions at centre of thickness were analysed. The EBSD technique allowed the degree of misorientation to be measured between points within

the bainitic structures with a length step greater than 0.1 μm. The minimum misorientation which can be reliably measured was taken as 2° and the misorientation between adjacent measurements which was greater than this value was considered to constitute a boundary [3].

Bainitic microstructures of modern high strength steels are typically very fine (typical lath widths of 0.1-0.5 μm and difficult to interpret quantitatively using conventional metallographic techniques. They can only be properly characterized using modern metallographic techniques based on high resolution scanning electron microscopes (SEM) and electron backscatter diffraction (EBSD). EBSD is a tool to quantify misorientation between different microstructure constituents and grains. The number and nature of boundaries in the microstructure obtained by EBSD mapping provides a means of distinguishing between different forms of bainitic ferrite [3].

As it was difficult to satisfactorily reveal the prior austenite grain structure using etching techniques, a computational reconstruction technique was applied to the EBSD results using Matlab supplemented with the MTEX texture and crystallography analysis toolbox [41]. Briefly, grain maps were initially assembled from the data sets with a grain boundary tolerance of 3-5 degrees. Subsequently, the parent austenite orientation map was reconstructed from this data with a two-step reconstruction algorithm. Firstly, the orientation relationship between the parent austenite and product ferrite phase was determined using the method proposed by Nyyssönen et al. [42] based on the Kurdjumov–Sachs (K–S) relationship [43] (i.e., $\{111\}_\gamma // \{110\}_\alpha$, $\langle 110\rangle_\gamma // \langle 111\rangle_\alpha$). In the second step, the grain map was divided into discrete clusters using the Markov clustering method [44] proposed by Gomes and Kestens [45]. The parent austenite orientation was then calculated for each cluster separately, resulting in a reconstructed austenite orientation map. The average misorientation between the reconstructed orientation for each cluster and the best fit for each individual grain was approximately 2 degrees, indicating a good fit for the reconstructed result. The full details for the reconstruction procedure have been described by Nyyssönen [46].

5.7 Heat affected zone simulation

Gleeble 3800 thermomechanical simulator was used to simulate the heat affected zone (HAZ) of investigated steels. The purpose was to simulate the coarse-grained zone of HAZ region (CGHAZ). Samples 10 x 10 x 55 mm in size were prepared for Gleeble simulations. The following simulation was applied: heating at 100 °C/s to 1300°C, followed by 50 °C/s to 1350 °C, holding at 1350 °C for 1 s and cooling using the cooling program with a cooling time from 800 to 500 °C ($t_{8/5}$) of 5 s and 15 s. After the simulation experiments, the Charpy V-notch tests were performed at temperatures of -40 °C and -60 °C, the hardness profiles through the HAZ area were measured using 10 kgs load (HV10) and microstructural characterization were performed using light optical microscopy.

6 RESULTS AND DISCUSSIONS

6.1 Austenite grain growth study

Average austenite grain size was about 50 µm in all Stage 1 steels at soaking temperature of 1100 °C. At soaking temperature of 1250 °C, average grain size was at around 500 µm or higher, comparatively larger than that of 1100 °C (Figure 13,14). At 1250 °C, 0.06Nb1Cr observed to have largest average grain size with least amount of Cr. Etching of Stage 2 materials to reveal prior austenite grain boundaries was difficult, therefore grain sizes of slab soaking were not determined.

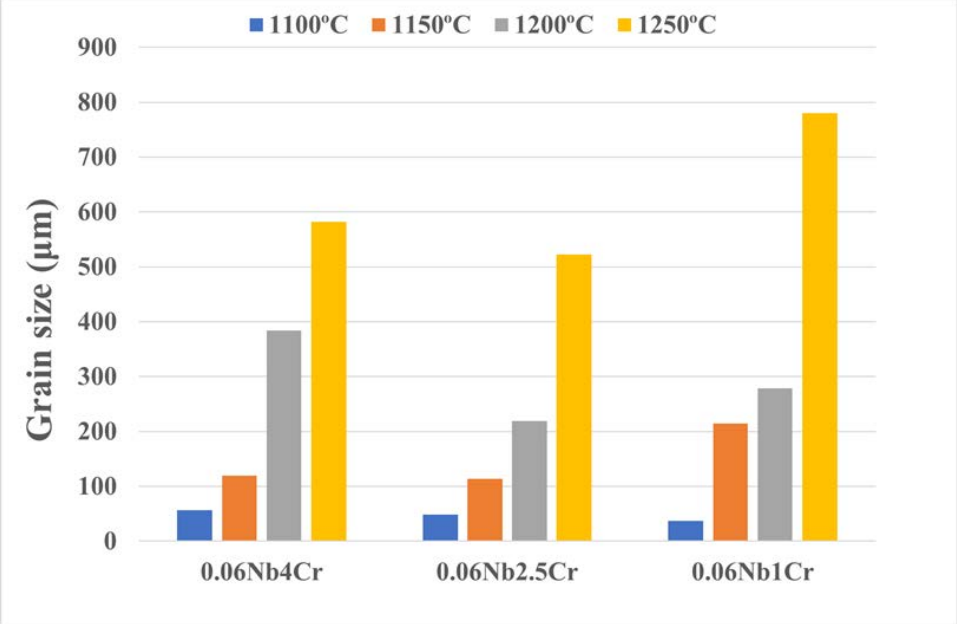

Figure 13. Average austenite grain sizes prior to hot rolling

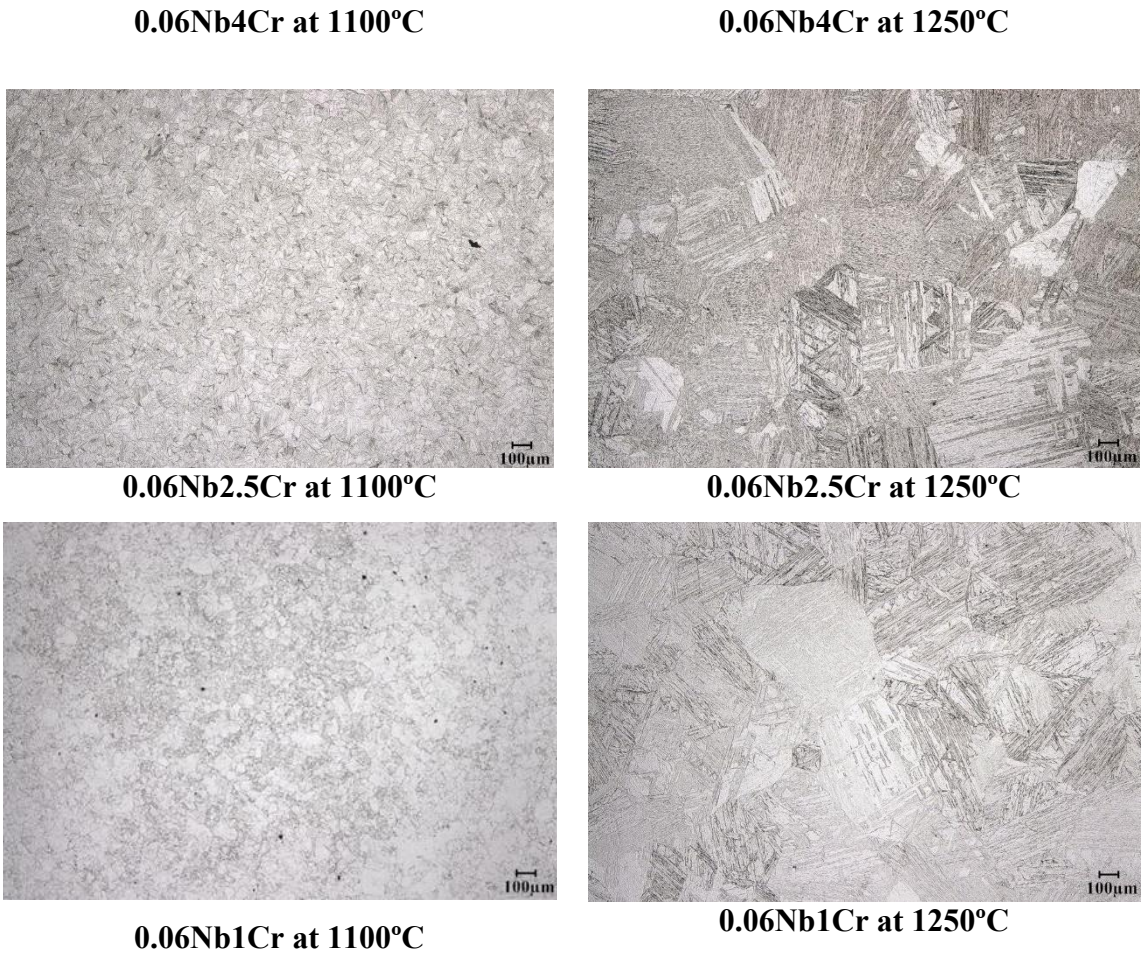

Figure 14. Microstructure after heating up to 1100 ºC and 1250 ºC of Stage 1 steels.

6.2 Microstructural characterization of hot-rolled materials

6.2.1 Effect of chemical composition on prior austenite morphology

Evaluation of prior austenite grain size (PAGS) was performed on metallographic specimens after etching with a saturated picric acid + hydrochloric acid + wetting agent solution to reveal the grain boundaries. Light optical microscope images of samples

etched with saturated picric acid solution to determine PAGs are presented in Figure 15. The steels with 4 % Cr were difficult to etch to reveal prior austenite grain boundaries (Figure 15). However, using EBSD data, the PAGs were reconstructed by using Matlab with MTEX software (Figure 16). The steel 0.06Nb1Cr and 0.06Nb2.5Cr shows signs of pancaking but was not present in 0Nb2.5Cr steel. Presence of 0.035 % niobium result in slight pancaking in 0.035Nb3.3Cr (Figure 15). From the reconstructed images, can be observed that 0.06Nb4Cr shows pancaking, while 0Nb4Cr is almost equiaxial austenite structure (Figure 16).

The grain refining effect of Nb is due mainly to delaying or preventing recrystallisation in the last hot forming steps. Flattened grains and a high dislocation density of the austenite enhance ferrite nucleation. By lowering the γ to α transformation temperature, Nb simultaneously enhances the ferrite nucleation rate and reduces the grain growth rate, and the combined effect leads to a particularly fine-grained transformation structure [33].

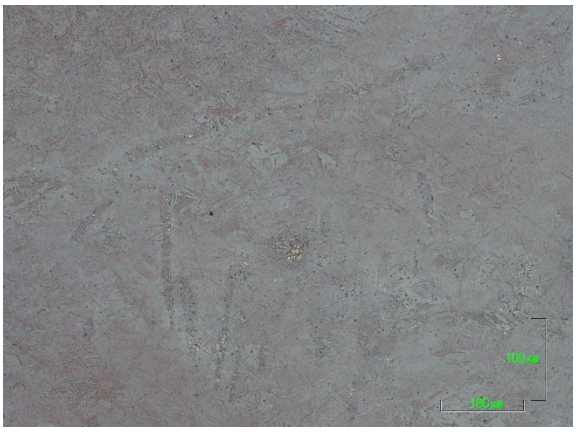

0.06Nb4Cr

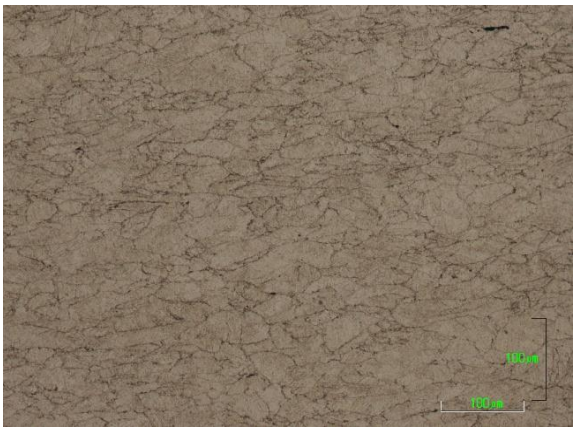

0.06Nb2.5Cr

0.06Nb1Cr

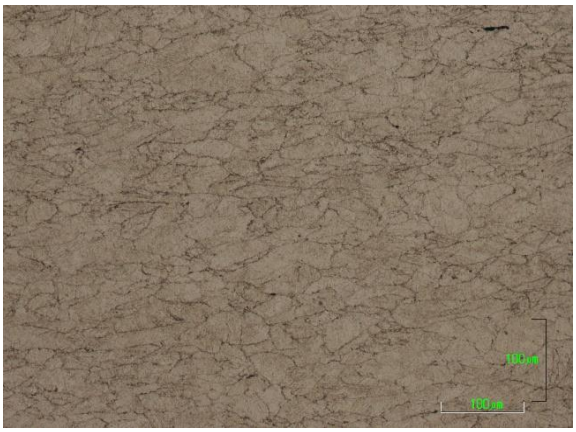

0.06Nb2.5Cr

0Nb4Cr

0.035Nb3.3Cr

Figure 15. PAGs after etching with saturated picric acid + hydrochloric acid + wetting agent.

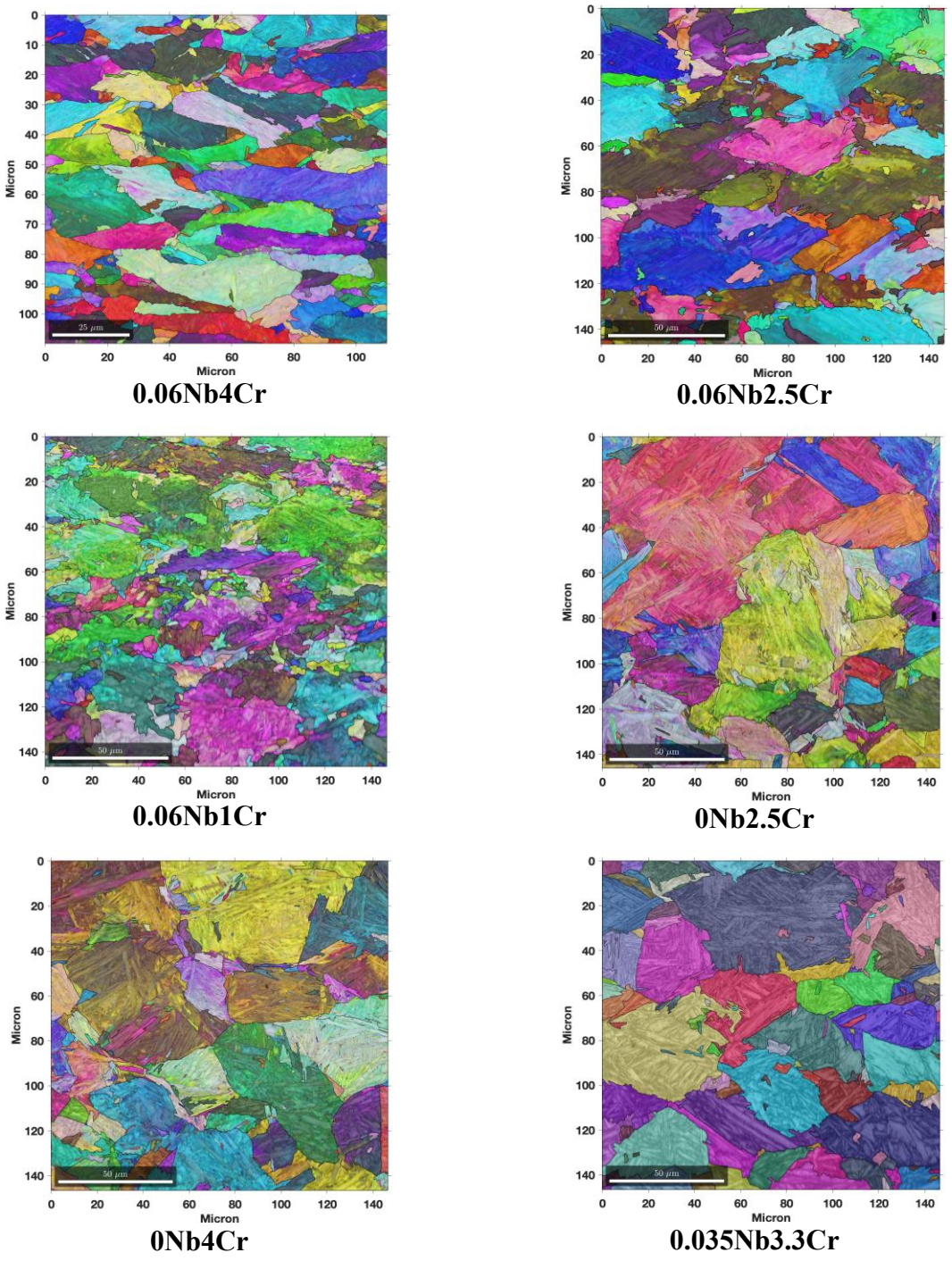

Figure 16. Images reconstructed from EBSD data using Matlab with MTEX toolbox.

6.2.2 The effect of alloying on the transformation microstructures

Samples from all six steels is etched with 2 % Nital to reveal general microstructure in Figure 17. Due to application of accelerated cooling technology, all the steel plates have various low temperature transformation microstructures granular bainite, upper bainite, coalesced bainite, lower bainite, as well as, quasi-polygonal ferrite. Microstructure characterization from quarter thickness and centerline is summarized in Table 2. Examples of different microstructure constituents observed are shown in Figures 18-22. EBSD image quality maps with high- (>15°) and low-angle (>2°) boundaries are presented in Figure 23. With the highest Cr content, microstructure consisted mainly lath-type structure such as upper bainite (UB) and lower bainite (LB), which, therefore, had smallest grain sizes. It was observed that all the steel has bainitic microstructure except for 0.06Nb1Cr and 0,06Nb2,5Cr which contains quasi-polygonal phase (Figure 21) which means that higher Cr is required to form fully bainitic microstructure.

Table 2. Microstructures that are present in each steel as quenched condition.

Steel	**Phases presents**
0.06Nb4Cr	GB, UB, LB, CB
0.06Nb2.5Cr	GB, UB, LB, QF
0.06Nb1Cr	GB, UB, QF, M/A films
0Nb2.5Cr	GB, UB, LB, CB
0Nb4Cr	UB, LB, CB
0.035Nb3.3Cr	UB, LB

GB = Globular Bainite, UB = Upper Bainite, LB = Lower Bainite, CB = Coalesced bainite, QF = Quasi-polygonal ferrite, M/A = Martensite/Austenite

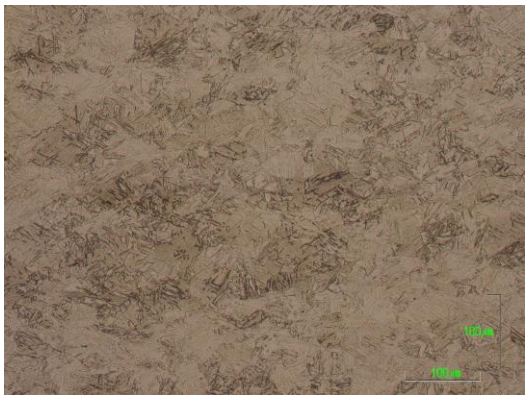

0.06Nb4Cr

0.06Nb2.5Cr

0.06Nb1Cr

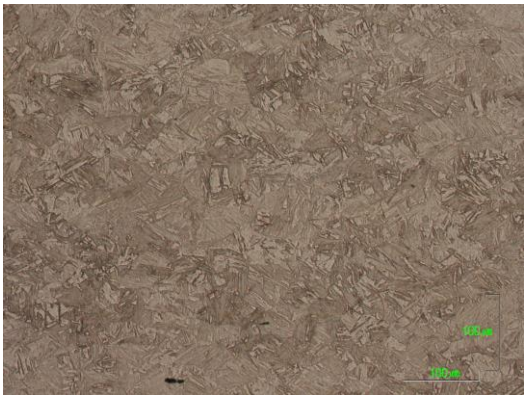

0Nb2.5Cr

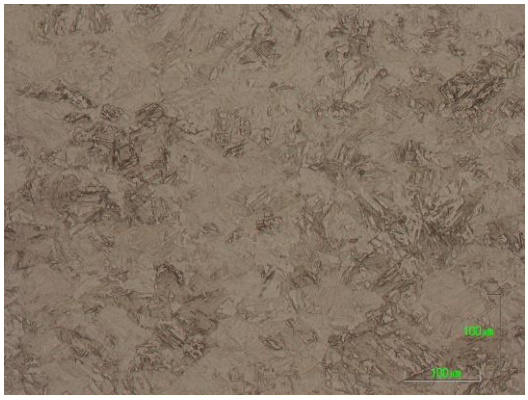

0Nb4Cr

0.035Nb3.3Cr

Figure 17. Typical microstructures of investigated steels after 2% Nital etching using light optical microscope.

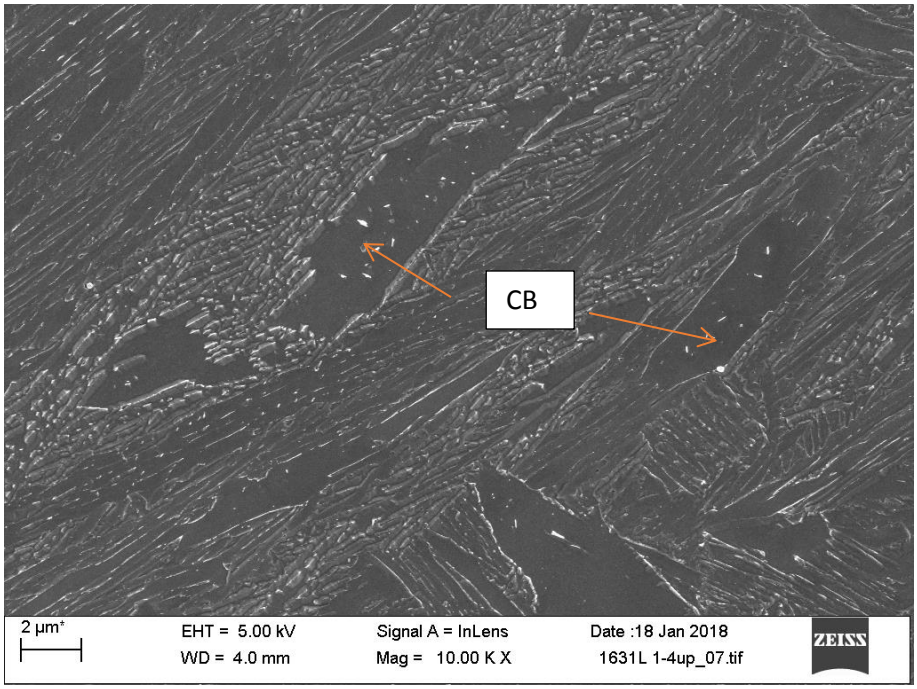

Figure 18. Coalesced bainite in 0.06Nb4Cr steel.

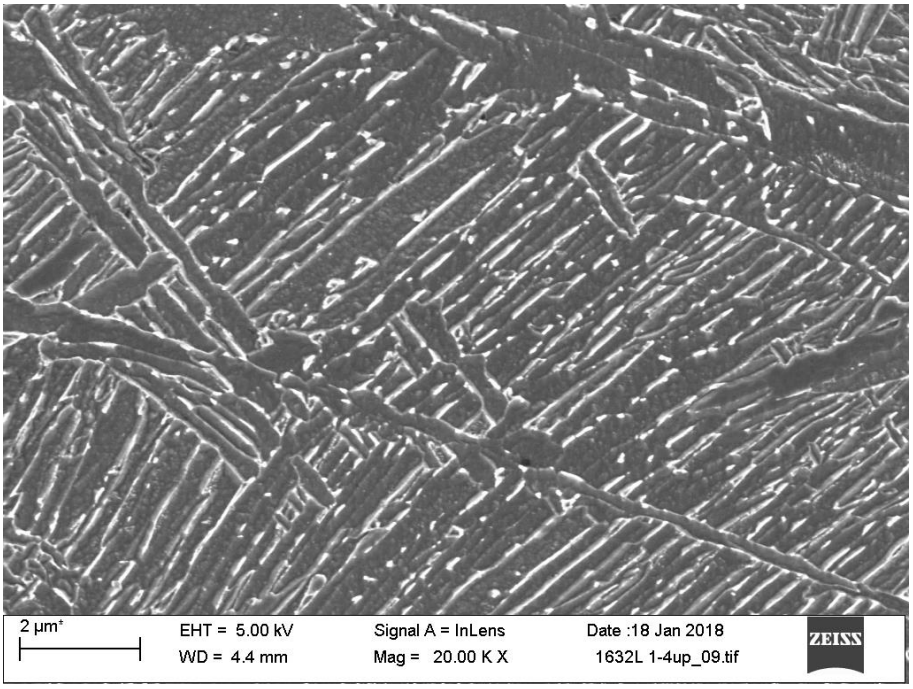

Figure 19. Lower bainite in 0.06Nb2.5Cr steel.

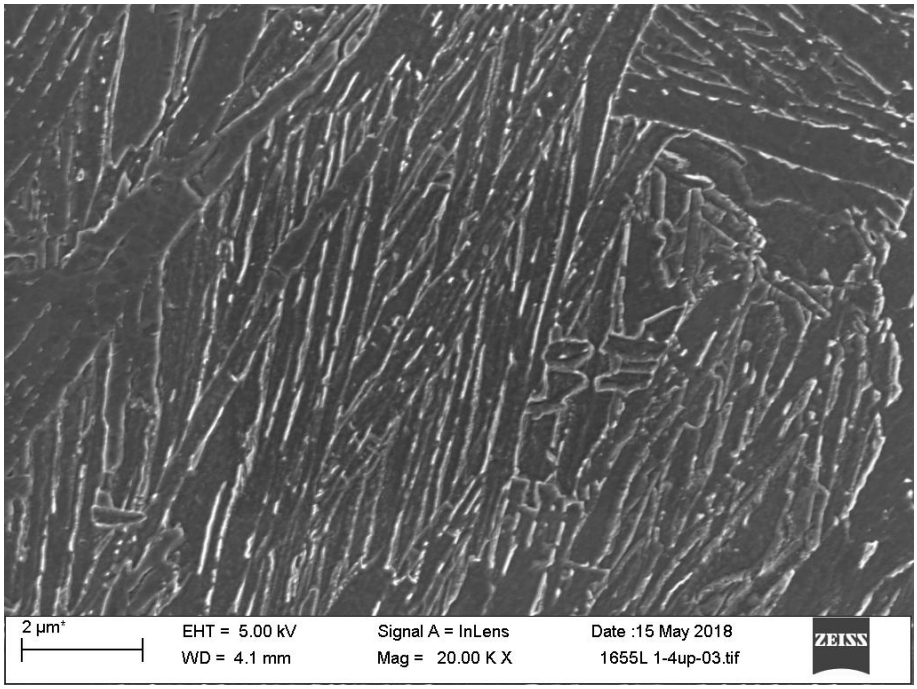

Figure 20. Upper bainite in 0Nb4Cr steel.

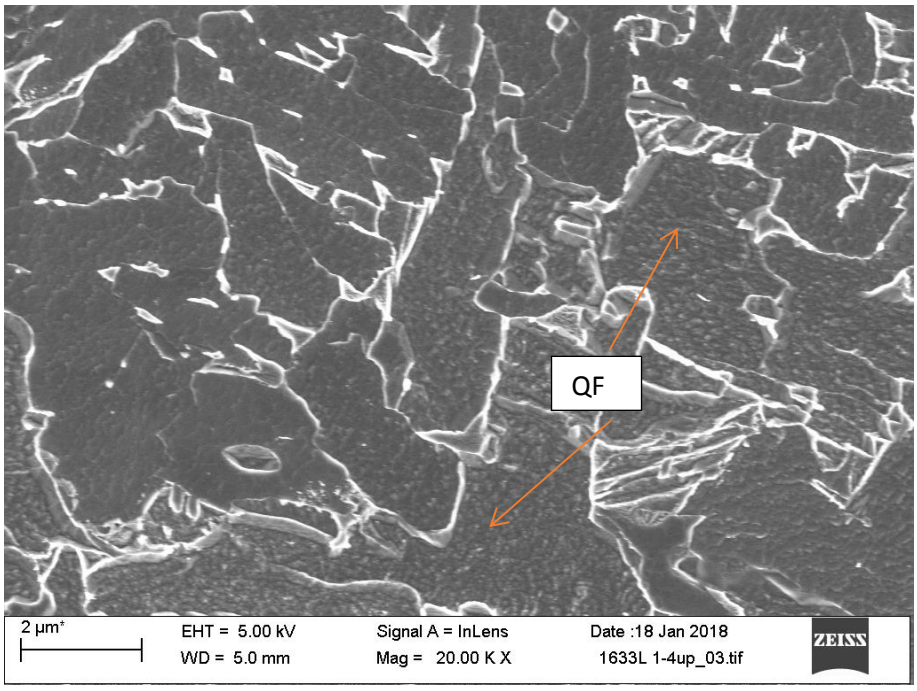

Figure 21. Quasi-polygonal ferrite in 0.06Nb1Cr steel.

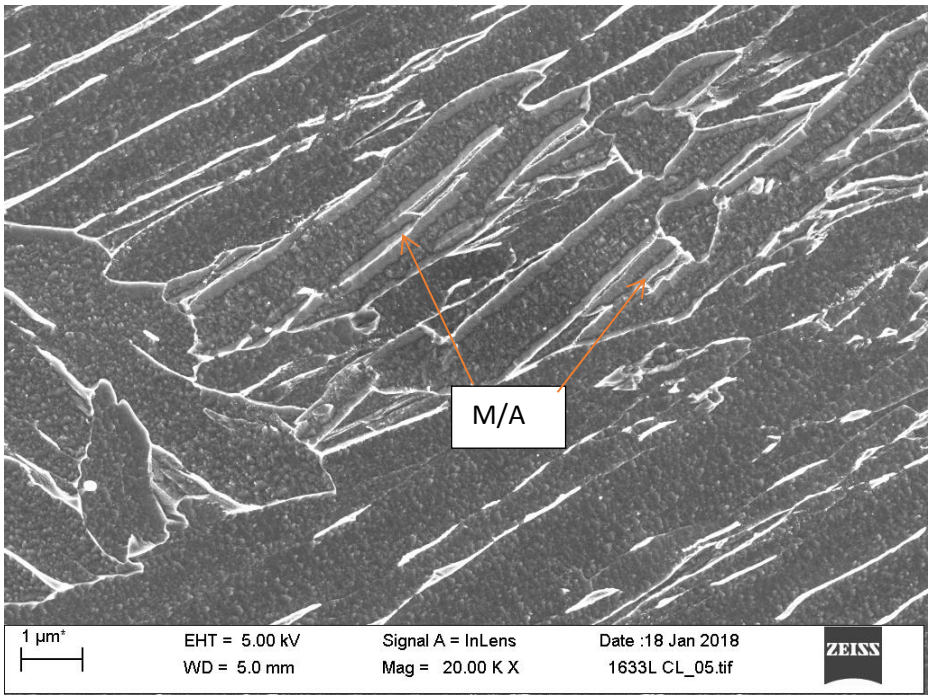

Figure 22. Granular bainite with films of M/A islands.

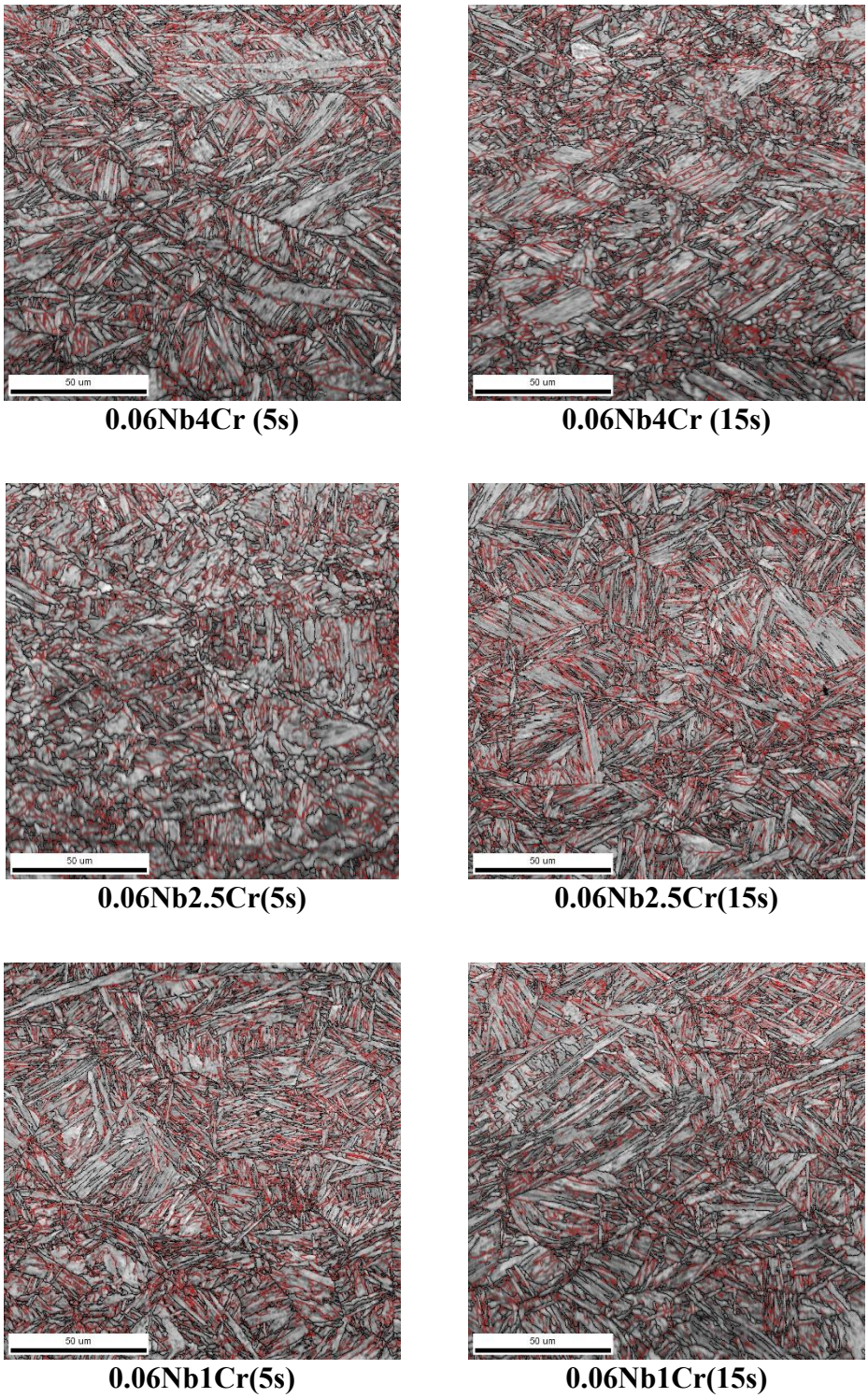

Figure 23. Grain boundary maps. High-angle boundary (15°-65°) = black line, low-angle boundary (2°-15°) = red line.

Grain misorientation distributions were determined using the EBSD data and are presented in Figures 21 and 22. Misorientation peaks at ~7.5° (sub-block boundaries), 16°, 52.5° and 59° (packet or/and block boundaries) are the result of different variants of the Kurdjumov-Sachs orientation relationship [43]. High peaks at ~9° (packet or/and block boundaries) are characteristics of lower bainite microstructures. Based on misorientation distributions, clear differences between some steels were apparent, which confirms the conclusion from the other microstructural investigations that of all the six steels. 0.06Nb4Cr, 0Nb2.5Cr, 0Nb4Cr and 0.035Nb3.3Cr were observed to consist UB and LB. They all have similar mechanical properties, hence identical graph (Figure 24). The upper bainite, consisting of carbide free ferrite with cementite particles at ferrite laths, showed two sharp peaks: the first at low-angle boundaries with misorientations range of 2-10°, the second at fewer number of high angle boundaries with misorientations in the range 50-60°. The lower lath-bainite, consisting of ferrite laths with interlath cementite, showed a low number fraction of low angle boundaries with misorientation angles between 2-10°, a sharp peak for high-angle boundaries with misorientations of 50-60° (Figure 24). [3]

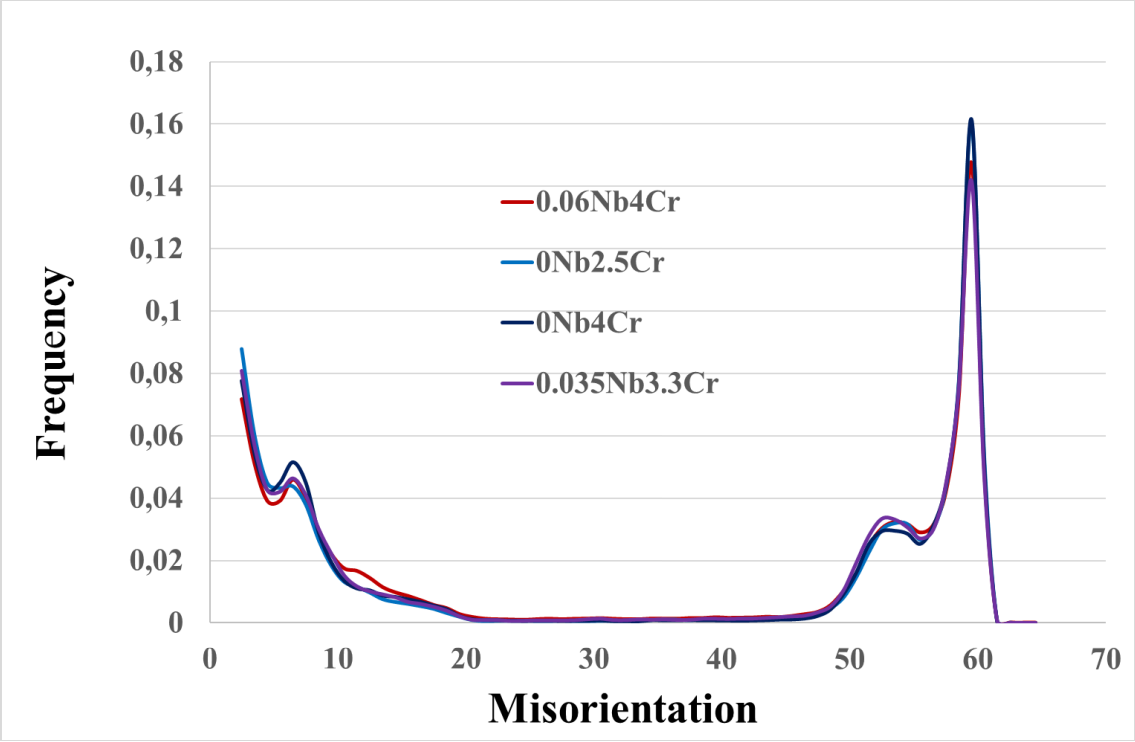

Figure 24. Grain boundary misorientation distributions of 0,06Nb4Cr, 0Nb2.5Cr, 0Nb4Cr and 0.035Nb3.3Cr (> 2°).

0.06Nb2.5Cr and 0.06Nb1Cr consists of granular bainite, consisting of carbide free irregular/acicular ferrite with retained austenite (or its transformation products) located in discrete regions or at the lath boundaries, confirmed by the distribution of grain misorientations was more random with a broad peak at about 45°. The existence of strong substructure produces a peak at low misorientations below 20° (Figure 25) [3]. 0.06Nb2.5Cr also contains lower bainite, therefore higher peak at 59°.

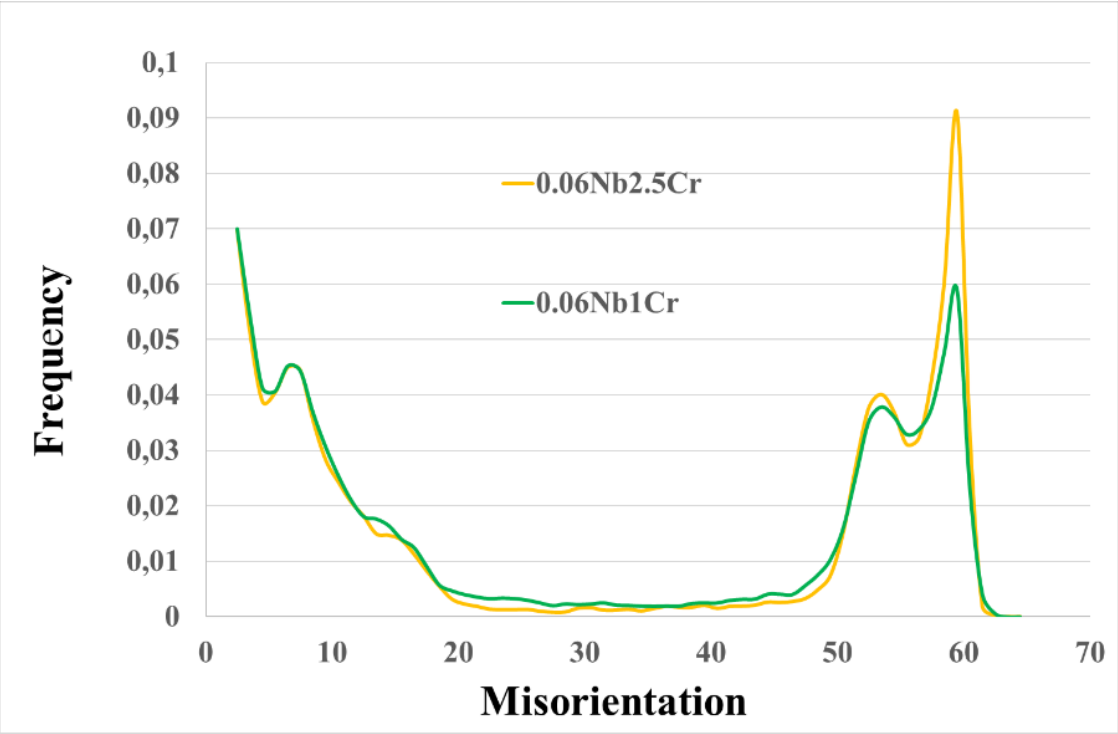

Figure 25. Grain boundary misorientation distributions of 0.06Nb2.5Cr and 0.06Nb1Cr (> 2°).

Effective grain and lath sizes were determined as equivalent circle diameter (ECD) values with low-angle (>2°) and high-angle boundary misorientations (>15°). Also 90 percentile effective high-angle grain sizes ($d_{90\%}$) were determined. Results are presented in Figure 26. Smaller effective grain and lath sizes were achieved by grain refinement due to alloying with Cr and Nb. As Cr content decreases, result in formation of quasi-polygonal ferrite in 0.06Nb2.5Crand 0.06Nb1Cr steels. As the ferrite content increased, lath and effective grain sizes became larger, in comparison to that seen in steels with 4%Cr

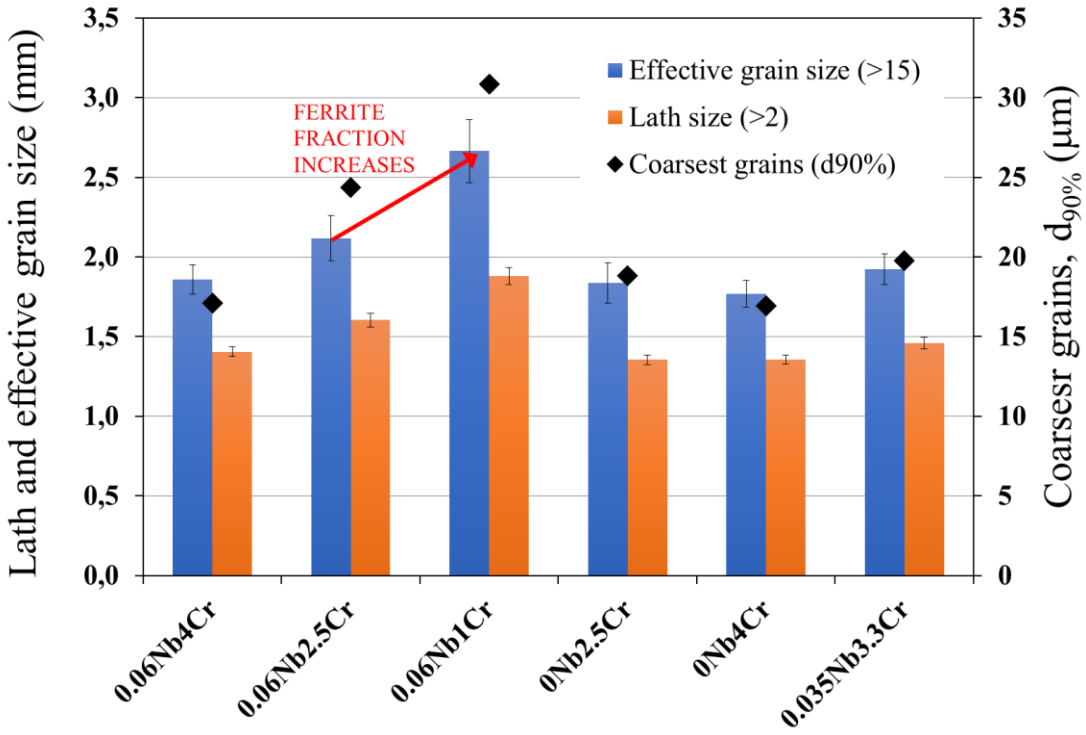

Figure 26. Effective grain, lath sizes and 90 percentile grain sizes of the effective grain size distributions.

6.2.3 The effect of microstructures and compositions on hardness

Hardness measurements were performed through the thickness of the samples using HV10 (Figure 27). The effect of quasi-polygonal ferrite (QF) on hardness can be seen on 0.06Nb2.5Cr and 0.06Nb1Cr from Figure 27. The hardness dropped significantly in the case of 0.06Nb1Cr steel, where large amount QF was formed in the microstructure (Figure 27). In addition, since Cr is a ferrite-stabilizing element [4], increase in Cr content reduced the amount of ferrite, which can be seen in increase in hardness values as shown in Figure 27. If finish rolling temperature of 880 °C is used, the higher hardness (~30 HV) level can be achieved without niobium, which can be seen Figure 28.

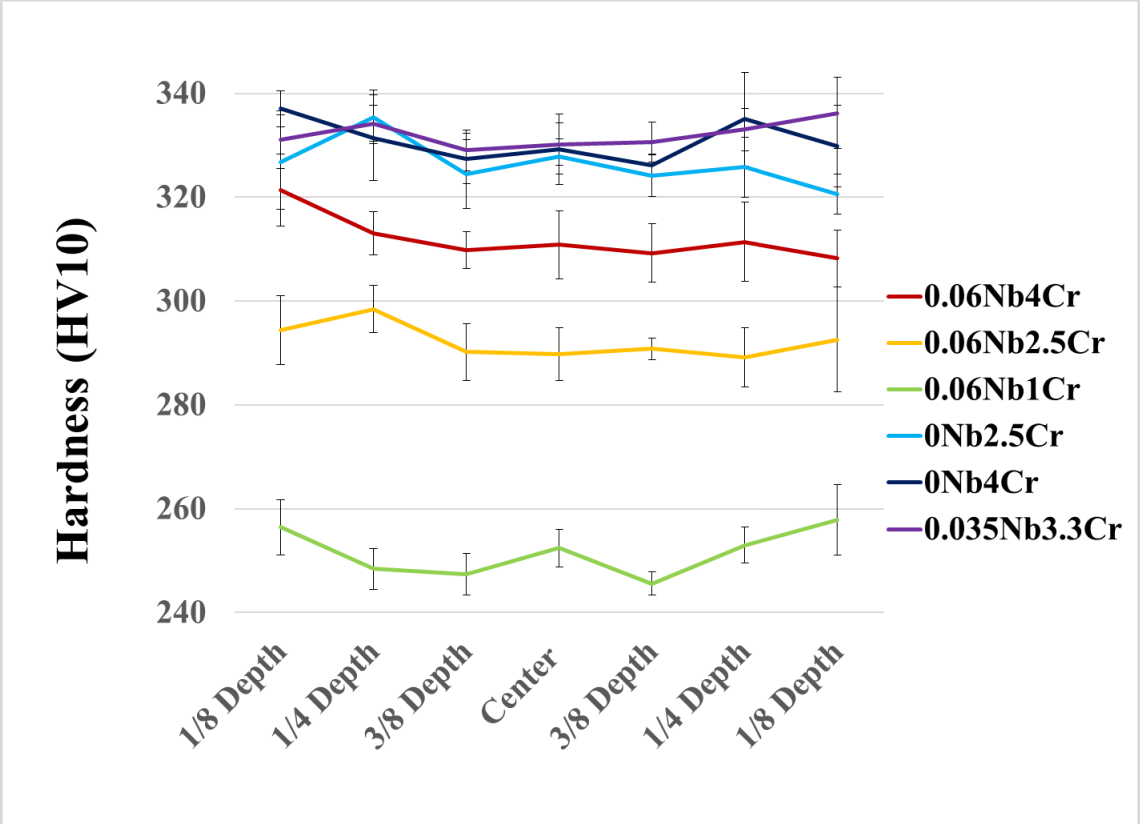

Figure 27. Hardness profile from surface to surface (HV10).

With the Cr increasing, the ferrite transformation was avoided, resulting in an increased bainite fraction. It was reported [7] that an increase in Cr content in the steel causes a separation of the bainite C- curve from the ferrite C-curve and extends the bainite phase field. The addition of Cr decreases the B_s and M_s, which contributes to the greater amount of bainite. Moreover, Cr addition enhances the hardenability of metastable austenite which can be seen from uniform hardness through the thickness (Figure 27) and increases the stability of austenite to ferrite. Therefore, more undercooled austenite can transform into lath like bainite in the Cr addition steel, which leads to the better properties of steel (Figure 28) [5].

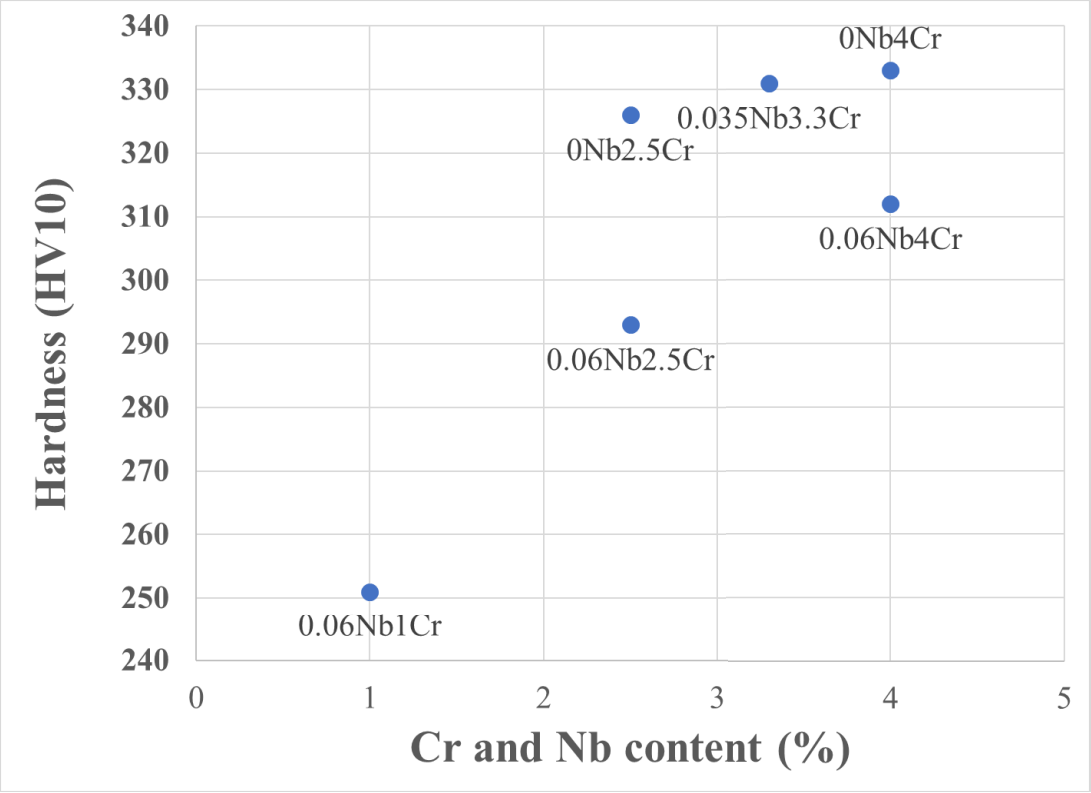

Figure 28. Effect of chromium and niobium on mean hardness.

6.3 The effect of compositions and microstructures on mechanical properties

Tensile properties are shown along with hardness values and T28J temperatures in Table 3. Transition curves were constructed based on Charpy V-notch test results. Standard 10x10x55 mm test samples were used from 12 mm thick rolled plates. The transition curves of steels are presented in Figure 30. Figure 31 presents the correlation between yield strength values and T28J transition temperature of investigated steels

In respect of the desired level of 700 MPa yield strength, 0.06Nb4Cr, 0Nb2.5Cr, 0Nb4Cr, 0.035Nb3.3Cr and 0.06Nb2.5Cr steels were able to demonstrate similar tensile properties as in the industrial production (Table 3). 0.06Nb4Cr, 0Nb2.5Cr, 0Nb4Cr, 0.035Nb3.3Cr and 0.06Nb2.5Cr steels, with the FRT controlled at 880 °C, were able to achieve yield strength of 700 MPa or above, and low transition temperature of around -80 °C, essentially due to the formation of fine bainitic structure and the absence of ferrite in the microstructure. Increase in Cr content observed to have positive effect on yield strength and ultimate tensile strength (Table 3). Even without presence of niobium, it is possible to achieve required 700 MPa yield strength with 880 °C FRT for 0Nb2.5Cr and 0Nb4Cr. Increased of chromium observed to be increasing the transition temperature (T28J) which is not a good effect.

But the 0.06Nb1Cr steel showed has lowest transition temperature of -118 °C which is a good property to have but has lowest yield strength (560 MPa) obviously as a consequence of the formation of quasi-polygonal ferrite, though the total elongation (A) was relatively higher (Table 3). The presence of quasi-polygonal ferrite and granular bainite with M/A islands seem to have significant effect on the impact toughness of 0.06Nb1Cr steel, which is better than the higher Cr contents containing steels, both in respect of higher upper shelf energy as well as lower T28J temperature, as displayed in Table 4 and Figure 30. A good toughness is known to be associated with a massive

ferrite structure like quasi-polygonal ferrite [6]. On the other hand, thin films of martensite-austenite (M/A) constituents present in lath-like granular bainite might adversely affect the impact toughness (Figure 22) [7].

Table 3. Tensile properties longitudinal to rolling direction of investigated steels.

Steel	YS(Mpa)	UTS(Mpa)	A %	HV10	YS/UTS	UTS*A	T28J(°C)
	Avg	Avg	Avg	Avg			RD
0.06Nb4Cr	780	982	12,5	312	0,79	12238	-78
0.06Nb2.5Cr	699	909	14,1	293	0,77	12852	-93
0.06Nb1Cr	560	756	17,2	251	0,74	13034	-118
0Nb2.5Cr	751	959	12,8	326	0,78	12303	-101
0Nb4Cr	808	1028	12,6	333	0,79	12957	-92
0.035Nb3.3Cr	775	989	11,9	331	0,78	11802	-101
S700MC	≥ 700	750-950	≥ 12				

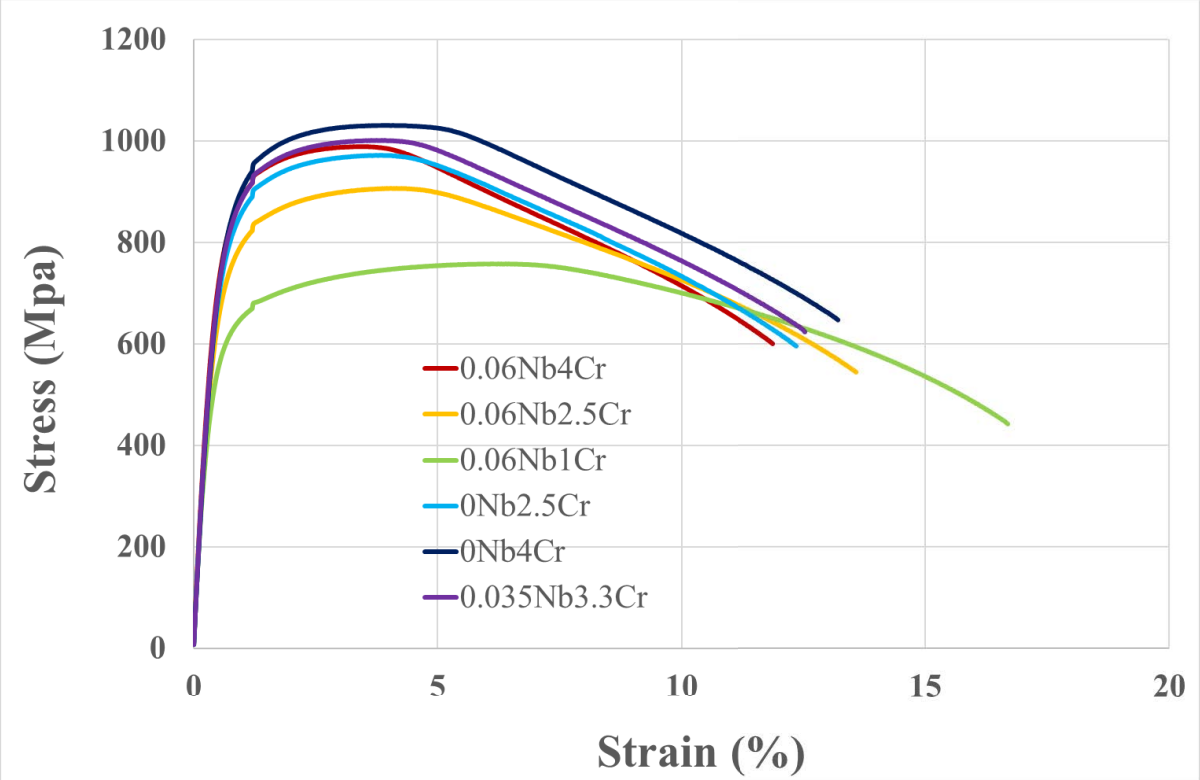

Figure 29. Stress-Strain curve of investigated steels.

Table 4. Charpy impact test results and T28J temperatures of investigated steels.

RD	20°C	0°C	-40°C	-60°C	-80°C	-100°C	-120°C	T28j(°C)
0.06Nb4Cr	208	184	123	60	12	17	13	-78
0.06Nb2.5Cr	215	216	122	54	33	25	22	-93
0.06Nb1Cr	244	274	221	172	100	101	16	-118
0Nb2.5Cr	220	218	148	138	60	22	38	-101
0Nb4Cr	190	200	150	46	44	16	17	-92
0.035Nb3.3Cr	206	224	127	93	62	26	12	-101

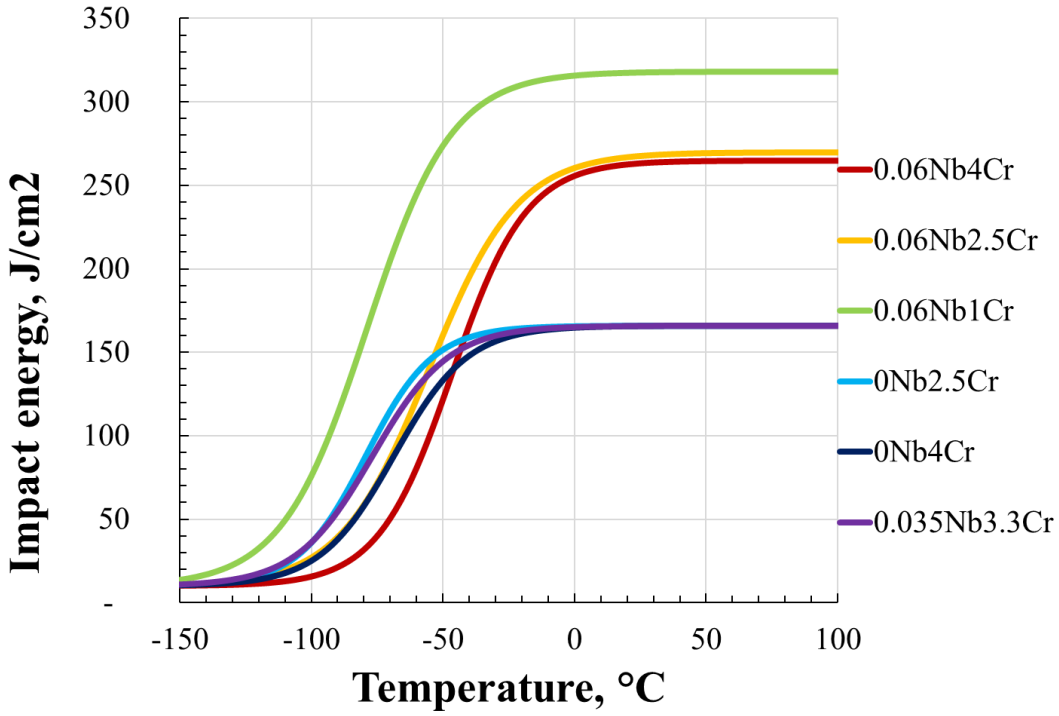

Figure 30. Transition curves based on Charpy V tests in rolling direction.

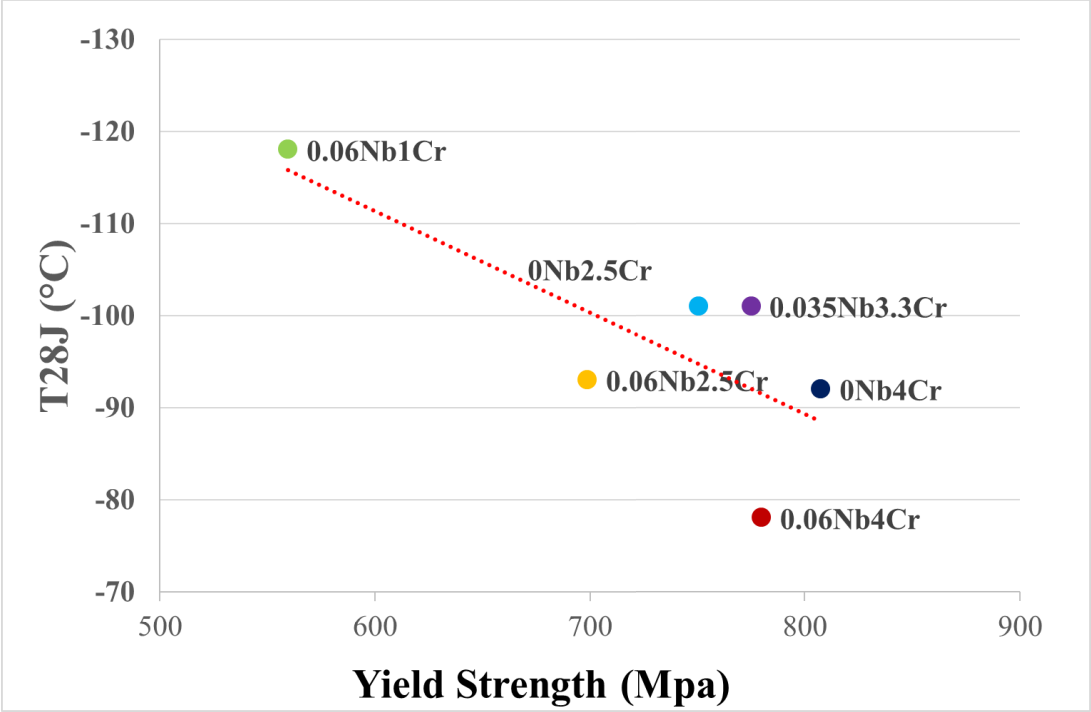

Figure 31. Yield strength vs. T28J transition temperature.

Regression analysis has been performed on the basic of niobium and chromium for yield strength ($R_{p0.2}$), tensile strength (R_m), total elongation (A %), uniform elongation (A_g), transition temperature (T28J) for both longitudinal and transverse direction using Minitab. In can be deduced from equation that increase in chromium and decrease in niobium can result in better mechanical properties.

The following equations 2-7 have been obtained:

1. $R_{p0.2}$ (yield strength) = 559,3 - 760 Nb + 69,14 Cr (2)
2. R_m (tensile strength) = 763,0 - 902 Nb + 72,73 Cr (3)
3. A % (total elongation) = 17,907 - 1,514 Cr (4)
4. A_g (uniform elongation) = 6,577 - 0,950 Cr (5)
5. T28J (longitudinal) = -135,74 + 154,0 Nb + 11,23 Cr (6)
6. T28J (transverse) = -159,1 + 698 Nb + 14,06 Cr (7)

6.4 The effect of inclusions on impact toughness

Inclusions analysis was carried out and it is clear that 0Nb4Cr is exceptional compared to other steel, the inclusion number density having nearly twice as many inclusions as in other steels (Figure 32a). When looking at the chemical composition of the inclusions it seems that the most inclusions in 0Nb4Cr belong to AlO class. AlO together with MnS+AlO made the majority of inclusions in all the studied steels. Pure MnS occurred also frequently in most of the steels (Figure 32b). These inclusions tend to elongate during the hot rolling making them long without increasing their area. Although 0Nb4Cr, contains more inclusions than other steels, it is impossible to correlate between inclusions and its effect on impact toughness but resulted in highest yield strength, tensile strength and hardness (Table 3).

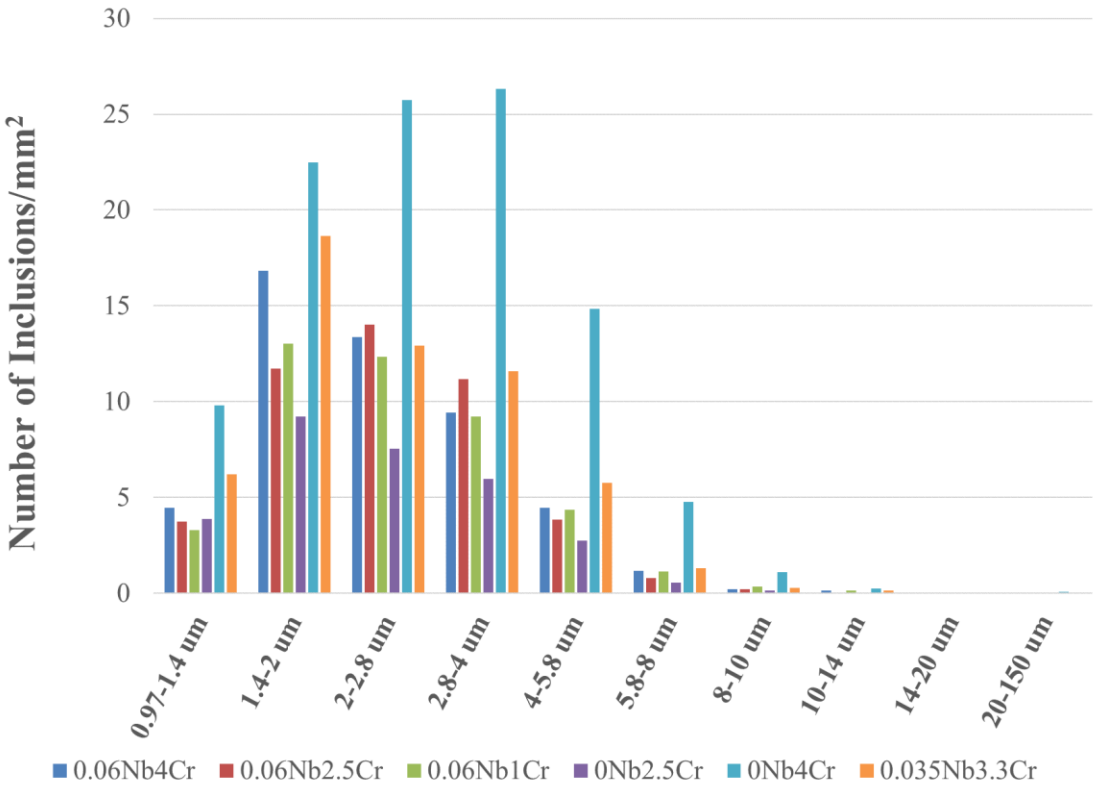

(a)

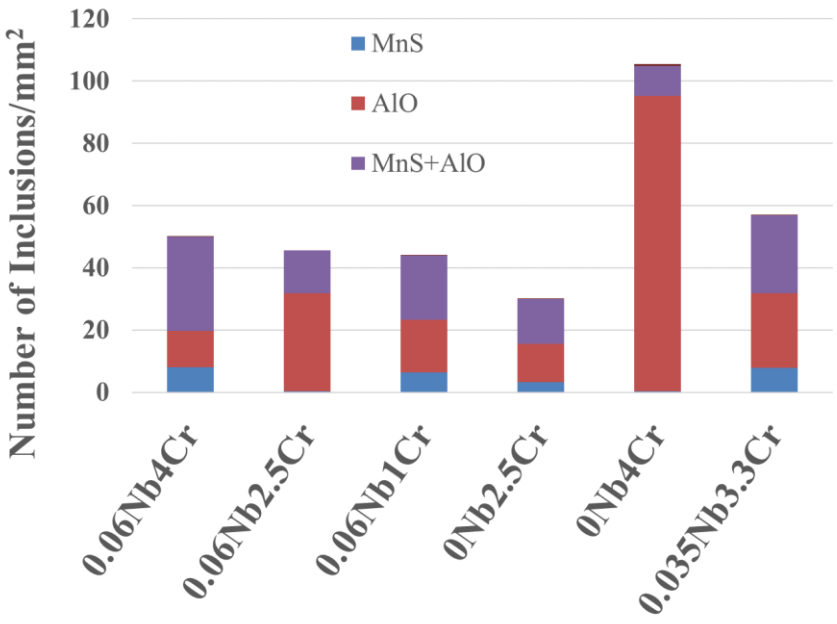

(b)

Figure 32. (a) Size distributions of inclusions and (b) number density of MnS, AlO and MnS+AlO coarse inclusions >4 μm of investigated steels.

6.5 HAZ simulation

Hardness measurements were performed through the simulated HAZ zones of the samples using HV10 procedure and are presented in Figure 33. Softening has occurred in most steel except for the steels 0.06Nb4Cr and 0.035Nb3.3Cr where softening is negligible. The highest softening occurred in 0.06Nb1Cr, 0.06Nb2.5Cr and 0Nb2.5Cr steels at the CGHAZ regions, especially with 0.06Nb2.5Cr and 0Nb2.5Cr steels with more softening occurring in samples with longer $t_{8/5}$ time (15 s).

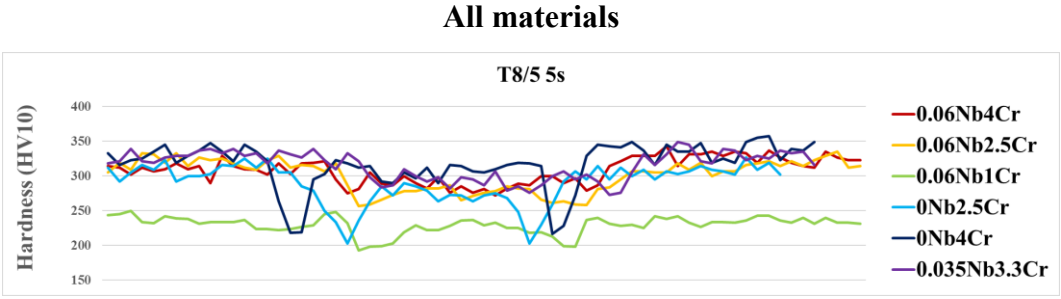

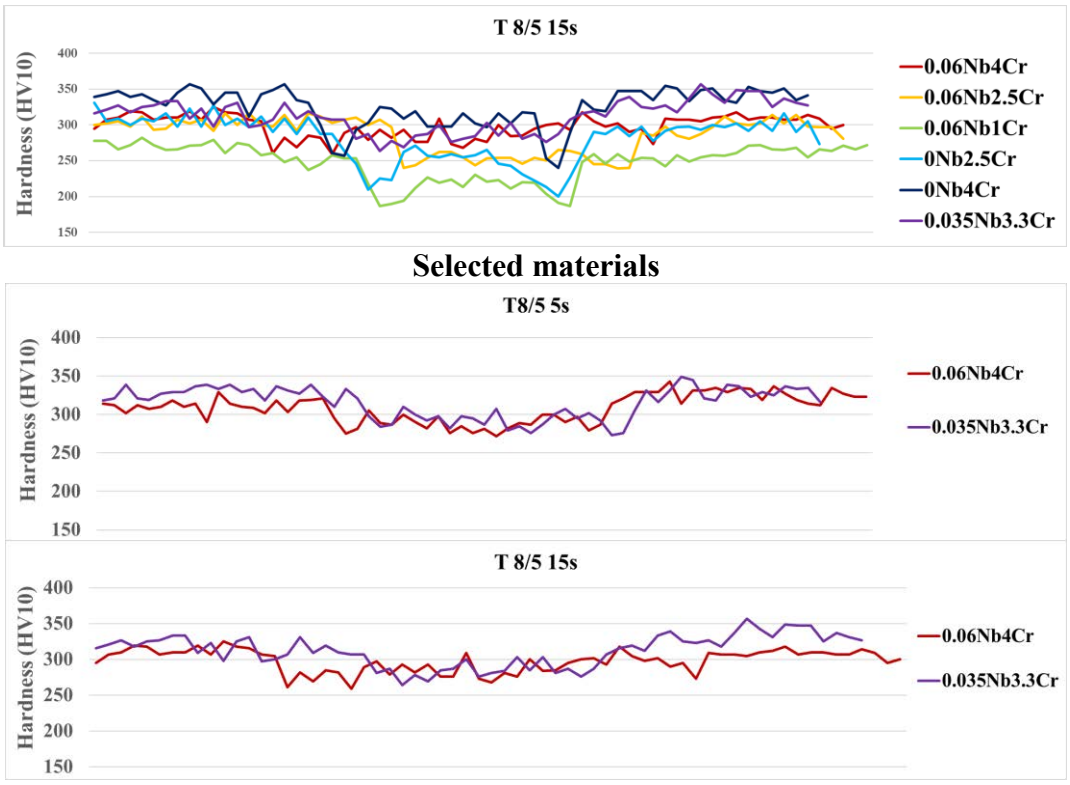

Figure 33**.** Hardness measurements through CGHAZ zones.

As can be seen from Figure 33, decrease in hardness of CGHAZ of 0.06Nb4Cr and 0.035Nb3.3Cr steels were negligible. Higher Cr content decreased the amount of softening in the HAZ region, especially with longer (15 s) $t_{8/5}$ –time due to an increased through-thickness hardenability. The average hardness of 0.06Nb4Cr and 0.035Nb3.3Cr steel in direct quenched condition was 312 and 331 HV, whereas the CGHAZ simulated samples with $t_{8/5}$ of 5 s and 15 s showed a marginally lower hardness of 287 and 290 HV (Figure 34). This suggests that even with a longer $t_{8/5}$ time of 15 s, it should be possible for the HAZ area to achieve mechanical properties nearly similar to the base metal.

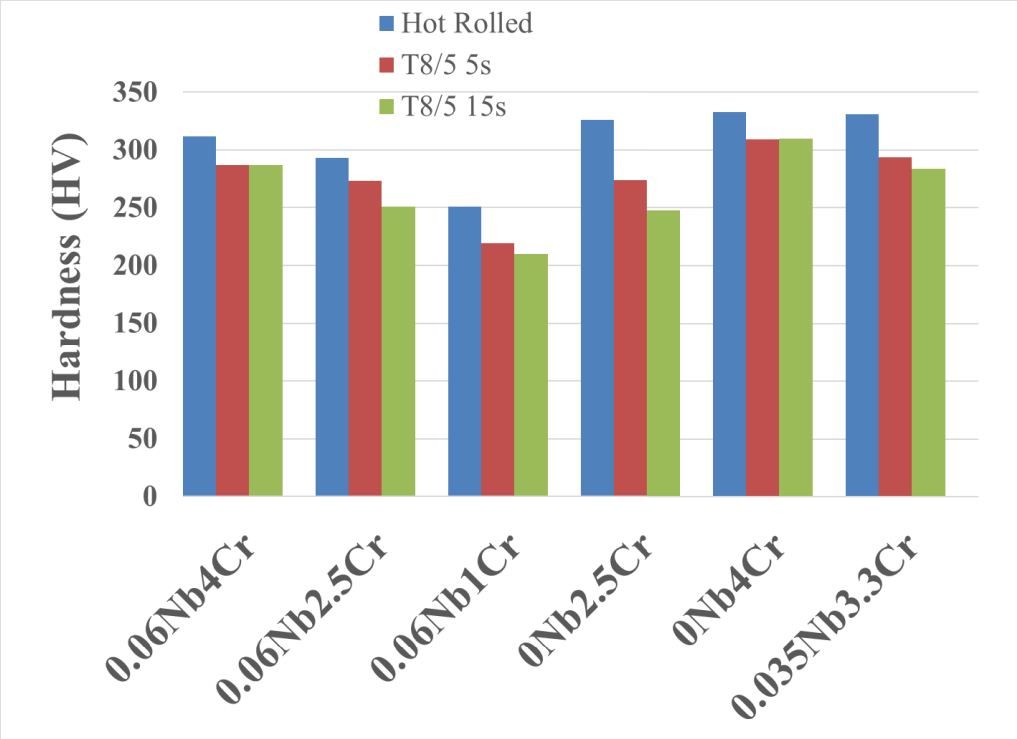

Figure 34. Comparison of harness as hot-rolled, $t_{8/5}$ 5 s and 15s.

The microstructures of CGHAZ simulated samples with $t_{8/5}$ = 5 s and 15 s cooling cycle are presented in Figure 35. Microstructures essentially consisted of mixtures of different bainite types and with small fractions of quasi-polygonal ferrite in 0.06Nb2.5Cr and 0.06Nb1Cr steels. With longer $t_{8/5}$ time (15 s), amount of quasi-polygonal ferrite was higher when compared with $t_{8/5}$ time (5 s) (Figure 35), 0.06Nb2.5Cr contains lower amount of quasi-polygonal ferrite than 0.06Nb1Cr due to higher Cr content.

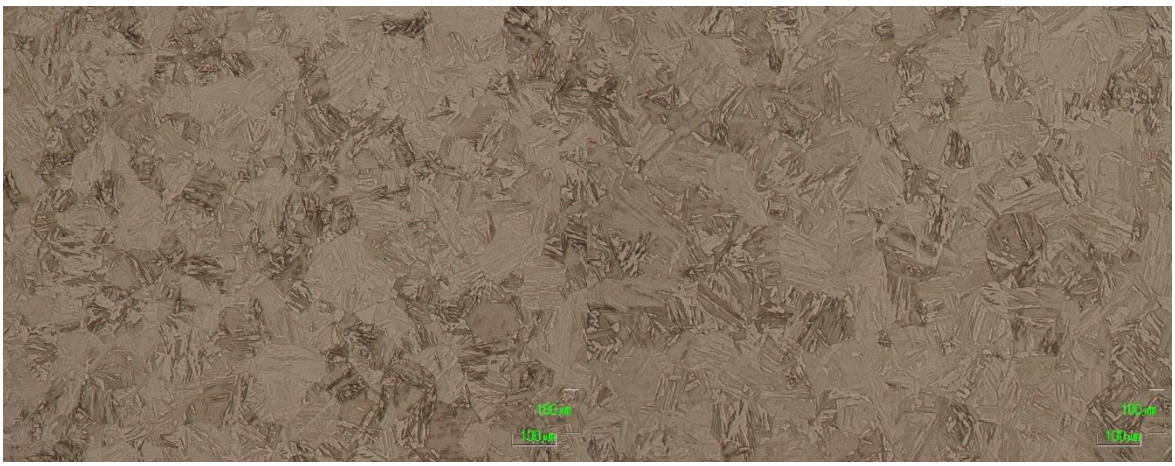

0.06Nb4Cr (5s) **0.06Nb4Cr (15s)**

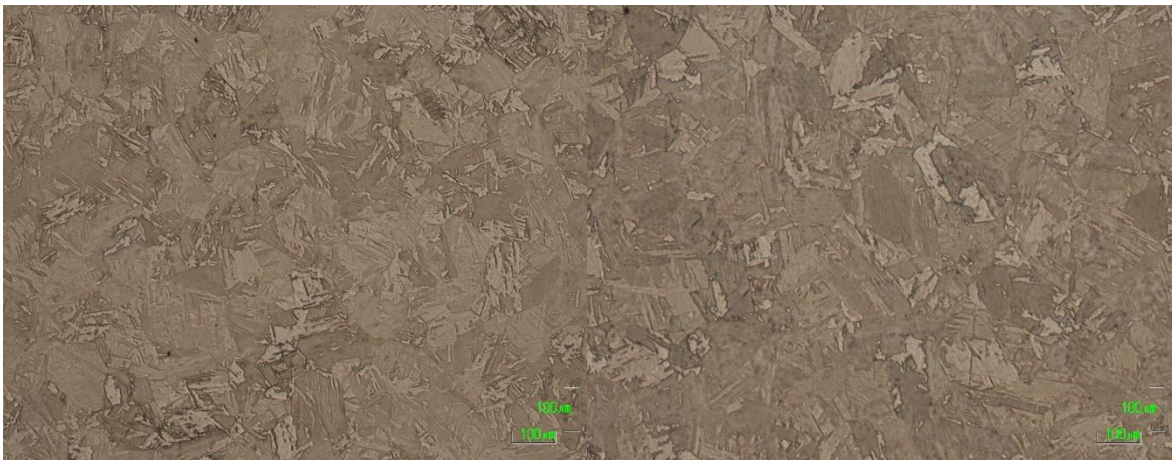

0.06Nb2.5Cr(5s) **0.06Nb2.5Cr(15s)**

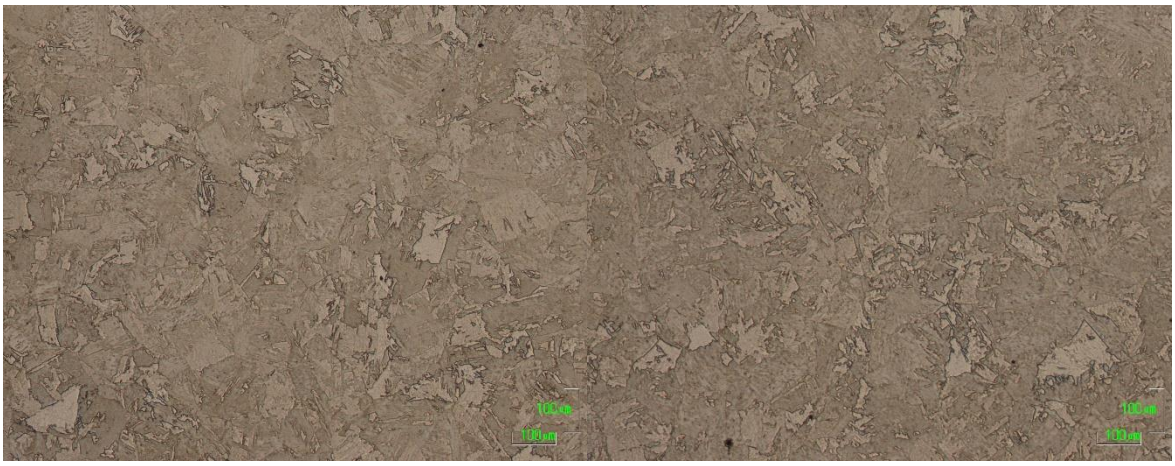

0.06Nb1Cr(5s) **0.06Nb1Cr(15s)**

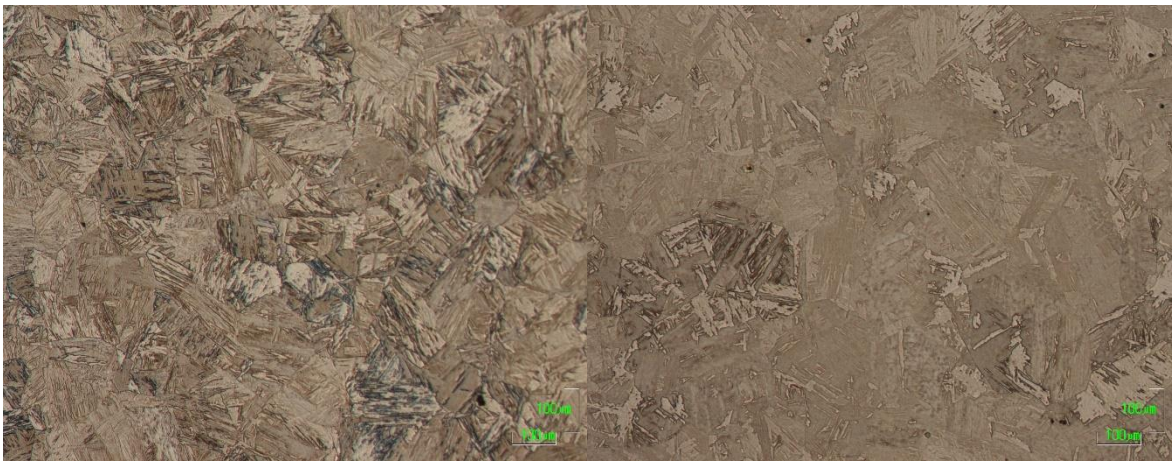

0Nb2.5Cr(5s) **0Nb2.5Cr(15s)**

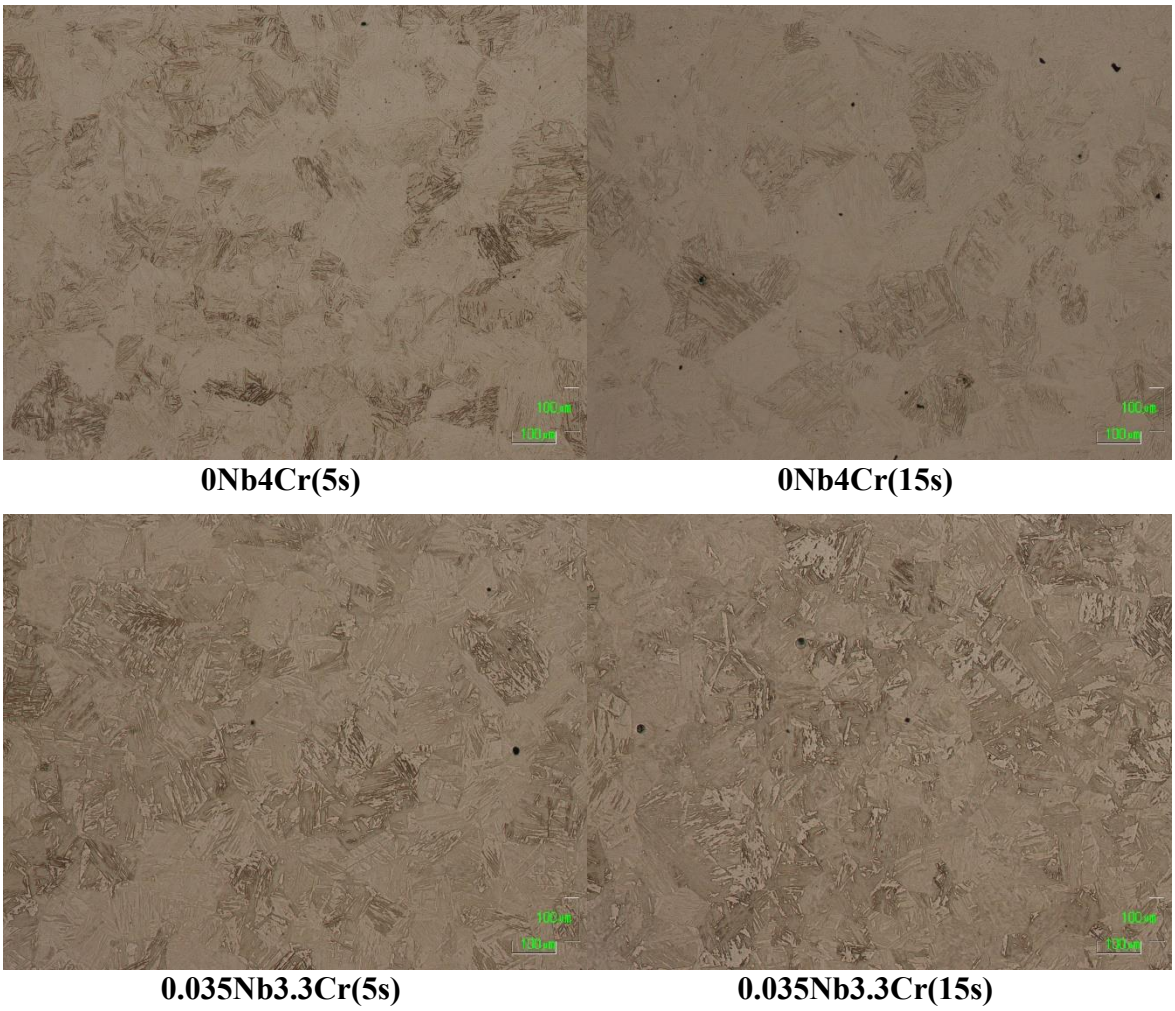

0Nb4Cr(5s) **0Nb4Cr(15s)**

0.035Nb3.3Cr(5s) **0.035Nb3.3Cr(15s)**

Figure 35. Microstructures of CGHAZ of investigated steels.

The Charpy V impact test data for CGHAZ samples at -40 °C and -60 °C were plotted in Figures 36 for both the cooling cycles corresponding to $t_{8/5}$ = 5 and 15 s. As expected, shorter $t_{8/5}$ time (5 s) corresponding to the higher cooling rates gave better impact toughness properties compared to the longer duration $t_{8/5}$=15 s samples (Figure 36).

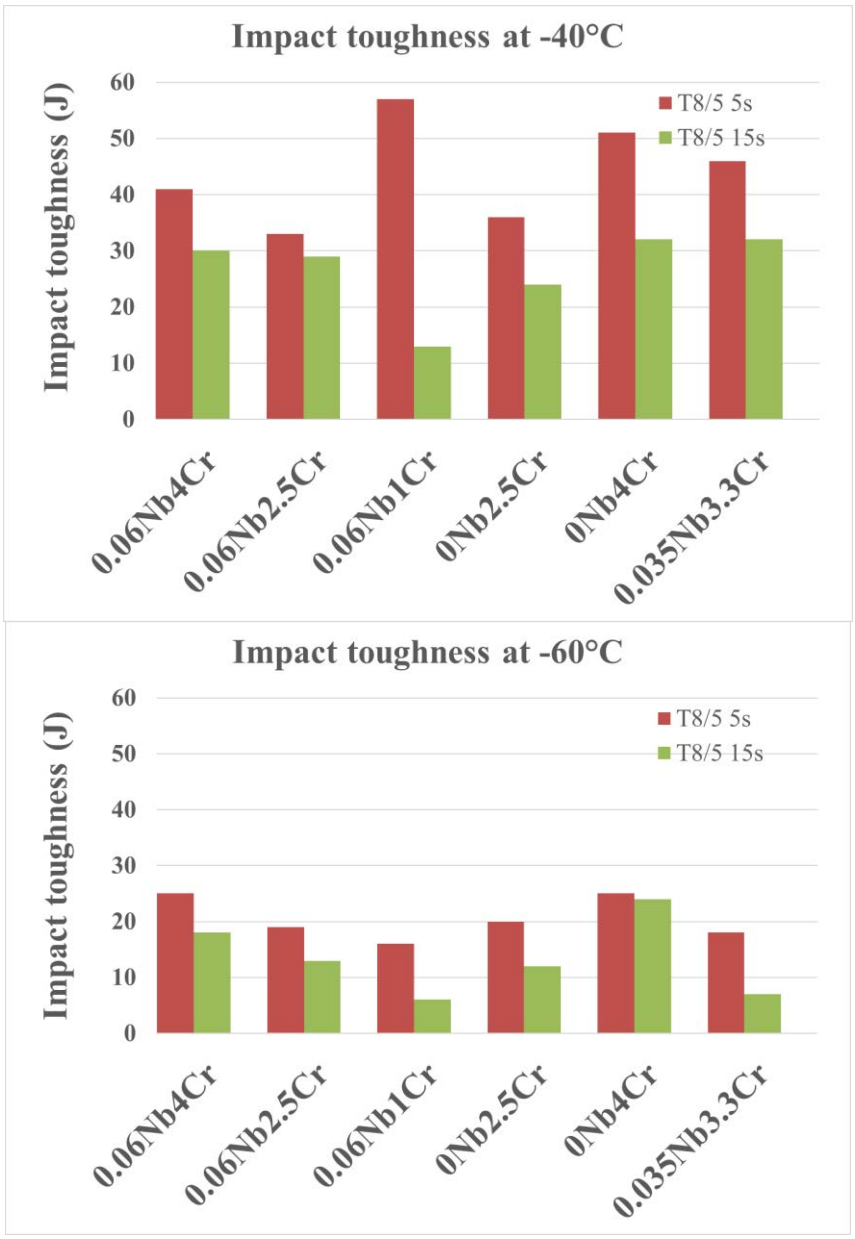

Figure 36. Charpy V-notch test results of steels after CGHAZ simulation tests.

7 CONCLUSIONS

The main aim of this thesis was to understand the effect of chromium and niobium on the microstructures and mechanical properties of low-carbon steel processed through TMCP rolling followed by direct quenching. The study also included weldability aspects

of these steels through Gleeble simulations. The thesis proposed high yield strength of the order of 700 MPa in these steels with good ductility and improved low temperature toughness in direct-quenched condition.

Due to difficulties in revealing prior austenite grain boundaries after slab reheating experiments, clear conclusions cannot be determined. However, there was no significant differences in prior austenite grain sizes between steels with different Cr contents. At 1250 °C, average prior austenite grain size was about 500 μm for all three Stage 1 steels, whereas at 1100 °C, average prior austenite grain size was about 50 μm.

Steels were hot rolled under rolling schedules to simulate rolling reduction from 60 mm thick steel slab to 12 mm thick steel plate in six passes to below the non-recrystallization temperature of 880 °C and direct-quenched in with the cooling rate of about 40-50 °C/s. The typical microstructures observed mainly mixtures of different type of bainite in all six steels exception of 0.06Nb1Cr steel which contained quasi-polygonal ferrite. Based on grain boundary misorientation distributions confirmed the microstructural observation from LOM and SEM investigation. Steels with 4 % Cr were not possible to reveal the PAGs with saturated picric acid + hydrochloric acid + wetting agent. Therefore, a computational reconstruction technique was applied to the EBSD results using Matlab supplemented with the MTEX texture to observe the grain structure. Steels with 0.06 % Nb revealed that pancaking occurred and the one with 0.035 % Nb showed slight pancaking of prior austenite grains. Steels without Nb were observed to have equiaxed prior austenite grain structure.

Niobium was observed to decrease the hardness. Increase in Cr content increased the hardness and uniform hardenability through the thickness of the plate was obtained. 0.06Nb1Cr have least Cr content which lead to formation of QF which in turn improved impact toughness and elongation but did not obtain required yield strength of 700 MPa. While the rest of the steels has with a yield strength of above 700 MPa in as-quenched condition and T28J transition temperature above or around -80 °C can be considered as good properties.

CGHAZ simulations showed that 0.06Nb4Cr and 0.035Nb3.3Cr steels have negligible softening and hardness is almost similar as base metal, which suggest with a longer t8/5 time of 15 s is possible for the HAZ area to achieve mechanical properties nearly similar to the base metal. In 0.06Nb2.5Cr and 0.06Nb1Cr steels more quasi-polygonal ferrite was formed with longer t8/5 time of 15 s compared to shorter t8/5 time of 5 s, which resulted in more softening in CGHAZ area. Due to higher cooling rate at t8/5 time of 5 s, compared to t8/5 time of 15 s, the impact toughness at -40 °C was higher than -60 °C, which was at or above 40 J/cm2 for all investigated steels. Although 0Nb4Cr have highest yield strength (Table 3), absence of Nb caused softening in CGHAZ.

Thus, the 0.06Nb4Cr and 0.035Nb3.3Cr steels have emerged as the potential candidate for 700 MPa grade steel proposed in this program owing to yield strength of above 700 MPa, T28J transition temperature in direct-quenched state below -80 °C. Also, in welded conditions, softening was negligible at both cooling cycle conditions (t8/5 = 5 and 15 s), which suggests that with a longer t8/5 time of 15 s, it is possible for the CGHAZ area to obtain mechanical properties as close to the base metal. Also, impact toughness of these two steels at -40 °C was relatively good (~45 J/cm2) in CGHAZ simulated samples.

FUTURE RESEARCH

Future research proposals can be summaries as follows:

- In order to control austenite grain growth during welding and improve toughness in CGHAZ, addition of titanium should be considered. Also, boron addition could be considered to improve the hardenability of steels.
- Gleeble studies for constructing CCT diagrams with lower cooling rate could be considered to provide more detailed information of behavior of composition on bainite formation.
- Multi-pass Gleeble simulation to provide more detailed effect on weldability of steels that meet the criteria.
- More detailed fracture surface analysis of 0.06Nb4Cr and 0.035Nb3.3Cr.

REFERENCES

[1] Xie H, Du LX, Hu J, Misra R D K. Microstructure and mechanical properties of a novel 1000 MPa grade TMCP low carbon microalloyed steel with combination of high strength and excellent toughness. Materials Science and Engineering: A. 2014.

[2] Bandyopadhyay P S, Ghosh S K, Kundu S, Chatterjee S. Evolution of Microstructure and Mechanical Properties of Thermomechanically Processed Ultrahigh.Strength Steel. Metallurgical and Materials Transactions A. pp 2742-2752, 2011.

[3] Yakubtsov LA, Poruks P, Boyd J D. Microstructure and mechanical properties of bainitic low carbon high strength plate steels, Materials Science and Engineering: A Volume 480, Issues 1–2, pp 109-116, 2008.

[4] Ormston D, Schwinn V, Hulka K, Development of Low Carbon Microalloyed Bainitic Steels for Structural Plate Applications. Materials Science Forum. MATER SCI FORUM. pp 573-580, 2005.

[5] Morris Jr., J W. The influence of grain size on the mechanical properties of steel, 2001.

[6] Zajac S, Schwinn C, Tacke K.H. Characterization and quantification of complex bainitic microstructures in high and ultra-high strength pipeline steels. Materials science forum, pp 387-394, 2005.

[7] Hee Jin L, Hae.woo L. Effect of Cr Content on Microstructure and Mechanical Properties of Low Carbon Steel Welds, Int. J. Electrochem. Sci. pp 8028-8040, 2015.

[8] Zhou LY, Liu, Y.Z.; Yuan, F.; Huang, Q.W.; Song, R.B. Effect of Cr on transformation of ferrite and bainite dual phase steels. J. Iron Steel Res. Int. pp 37–41, 2009.

[9] Ginzburg V. B.,Metallurgical design of flat rolled steels. Marcel Dekker, Inc. USA. 2005.

[10] Hashmi S. (2014) Comprehensive Materials Processing. Elsevier.

[11] Krauss G, Thompson S W. Ferritic Microstructures in Continuously Cooled Low. and Ultralow.carbon Steels. ISIJ international pp 937–945, 1995.

[12] Bhadeshia H. Materials Science Forum Vols 783.786 pp 2129–2135, 2014.

[13] Tian X, Yong L, Qun W, Zhao.dong W, Guo Dong. Effects of Ultra Fast Cooling on Microstructure and Mechanical Properties of Pipeline Steels. Journal of Materials Engineering and Performance, 2015.

[14] Yajima L.,.,'Extensive Application of TMCP.manufactured High Tensile Steel Plates to Ship Hulls and Offshore Structures' Mitsubishi Heavy Industries Technical Review Vol 24 No. 1, 1987.

[15] Singh S B, Bhadeshia H K D H. Mater. Sci. Technol. 14 pp 832, 1998.

[16] Nishioka K. Thermomechanical Proc. Steels. London, UK. pp 3, 2000.

[17] Honeycombe R W K. Steels, Microsrructure, and Properties, Edward Arnold Publishers, Ltd. 1981.

[18] Tanaka, T., Tabata, N., Hatomura, T., and Shiga, C., "Three Stages of the Controlled Roiling Process," Microalloying '75, Proceedings of an International Symposium on High.Strength, Low.Alloy Steels, pp 107-119, 1977.

[19] J.C. Ion J.C., K.E. Easterling K.E., M.F. Ashby M.F.A second report of microstructure and hardness heat-affected zones Acta Metallurgica, 32 (11), pp. 1949-1962, 1984.

[20] Impomet Oy. Valmistushitsaus, https://www.impomet.com/content/download /1728/20453/file/Valmistushitsaus.pdf

[21] Bramfitt B. L., Speer J. G.: A Perspective on the Morphology of Bainite, Metallurgical Transactions A, Vol. 21A, pp 817-829, April 1990.

[22] Zajac S., Morris P, Dierick P, Matera S. Technical Steel Research, Report EUR 21245EN, Luxembourg, pp 10, 2005.

[23] Hwang S. K., Martensitic Steels and Bainitic Steels. Inha Univ. 2001.

[24] Bhadeshia H K D H. Bainite in Steels. 2nd edition. IOM Communications Ltd. UK. 2001.

[25] Caballero F G, Bhadeshia H K D H, Mawella K J A, Jones D G, Brown P. Design of novel high strength bainitic steels. Mater Sci Technol. Design of novel high strength bainitic steels 2001.

[26] Wang J P, Yang Z G, Bai B Z, Fang H S. Grain refinement and microstructural evolution of grain boundary allotriomorphic ferrite/granular bainite steel after prior austenite deformation. Materials Science and engineering A369, pp 112-118, 2004.

[27] Wilson E A. Ferritic microstructures in continuously cooled low- and ultralow-carbon steels, ISIJ Int., 34 1994.

[28] Suikkanen P. Development and processing of low carbon bainitic steels. Acta Univ. Oulu. C 340, 2009.

[29] Garcia C I. Transformation strengthening of MA steels. Proceedings of the International Conference on “Microalloying ’95”, Pittsburgh, Pennsylvania, USA, 11–14 June, Iron and Steel Society, Warrendale, Pennsylvania, USA: pp 365–375, 1995.

[30] Yue s., “Thermomechanical Processing of Ferrous Alloys,” in ASM Handbook Metalworking: Bulk Forming, vol. 14 A, pp 286–296, 2005.

[31] Cuddy L., “Grain Refinement of Nb Steels by Control of Recrystallization During Hot Rolling,” Metallurgical Transactions A, vol. 15A, pp 87–98, 1984.

[32] Okaguchi S, Hashimoto T, Ohtani H. THERMEC, Japan, pp 330, 1998.

[33] Gupta C. K. and Suri A. K., “Extractive Metallurgy of Niobium,” CRC press, pp 21–23, 1994.

[34] Gulyayev A. P., Effect of chromium and nickel on toughness of steel, Metal Science and Heat Treatment of Metals, 1962, Volume 4, Number 11-12, 1962.

[35] Gaye H. Inclusion formation in steels.The making shaping and treating of steel, casting volume.11th ed. Pittsburgh, PA: AISE; 2003.

[36] Sauveur A. Metallography and heat treatment of iron and steel. 4th ed. New York, NY: McGraw-Hill; 1935.

[37] Srivastava A, Ponson L, Osovski S, Bouchaud E, Tvergaard V,Needleman A. Effect of inclusion density on ductile fracture toughness and roughness. J Mech Phys Solids pp 62–79, 2014.

[38] Pineau A, Benzerga AA, Pardoen T. Failure of metals I: brittle and ductile fracture. Acta Mater 107:424–83, 2016.

[39] Bertrand C, Molinero J, Landa S, Elvira R, Wild M, Barthold G,et al. Metallurgy of plastic inclusions to improve fatigue life of engineering steels.;30(2):165–9, 2003.

[40] Charpy impact test on metallic materials. Test method (V- and U-notches)

[41] Bachmann F., Hielscher R., Schaeben H., Grain detection from 2d and 3d EBSD data specification of the MTEX algorithm, Ultramicroscopy. 111 pp 1720–1733, 2011.

[42] Nyyssönen T., Isakov M., Peura P., Kuokkala V.-T., Iterative Determination of the Orientation Relationship Between Austenite and Martensite from a Large Amount of Grain Pair Misorientations, Metall. Mater. Trans. A. 47 pp 2587–2590, 2016.

[43] Kurdjumow G., Sachs G., Uber den Mechanismus der Stahlhärtung, Zeitschrift Fur Phys. 64 pp 325–343, 1930.

[44] Van Dongen S., Graph Clustering by Flow Simulation, University of Utrecht, 2000.

[45] Gomes E., Kestens L.A.I., Fully automated orientation relationship calculation and prior austenite reconstruction by random walk clustering, IOP Conf. Ser. Mater. Sci. Eng. 82 pp 12059, 2015.

[46] Nyyssönen T., Quenching and Partitioning of High-Aluminum Steels, Tampere University of Technology, 2017.

Appendix 1: Band contrast and inverse pole figure maps of investigated steels.

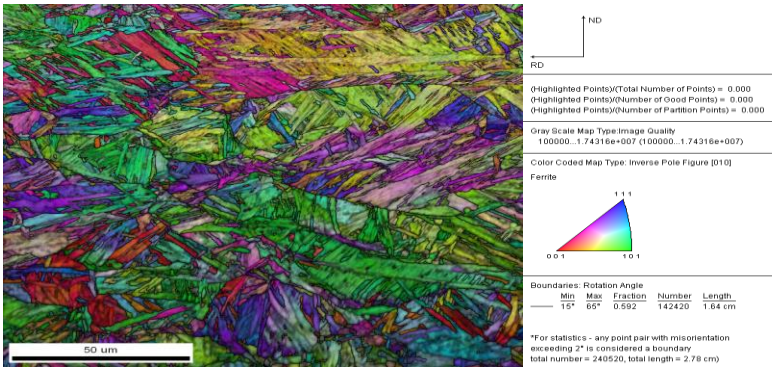

0.06Nb4Cr

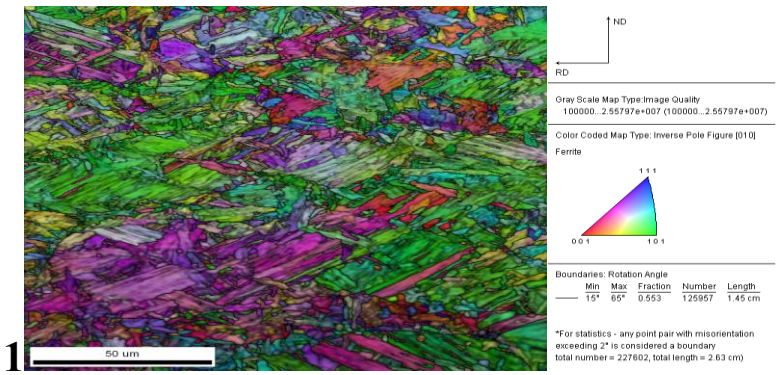

0.06Nb2.5Cr

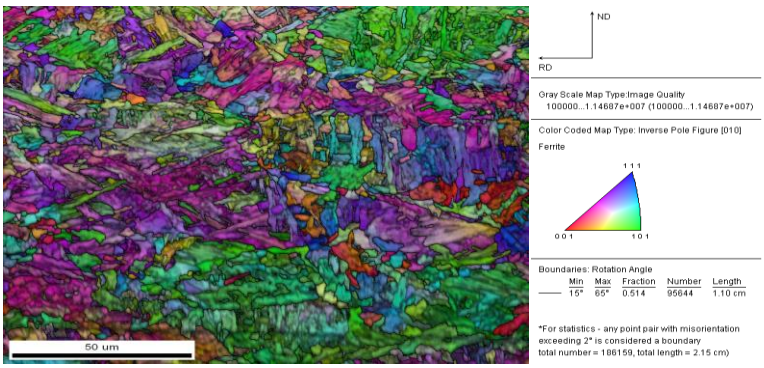

0.06Nb1Cr

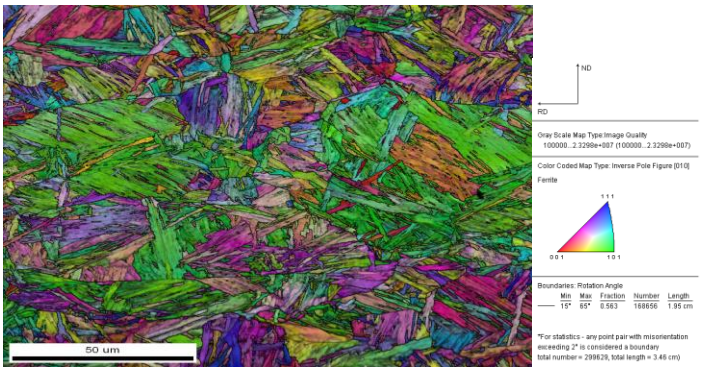

0Nb2.5Cr

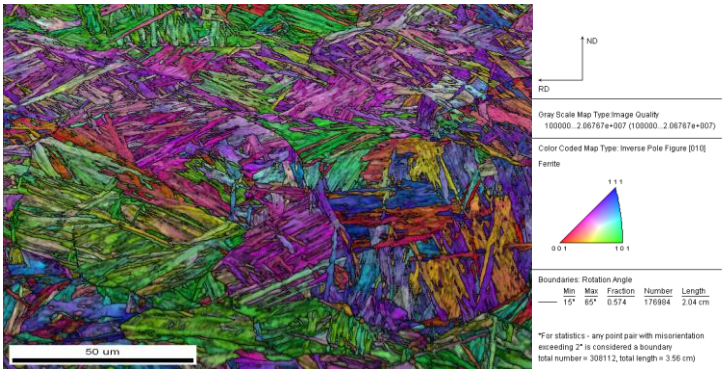

0Nb4Cr

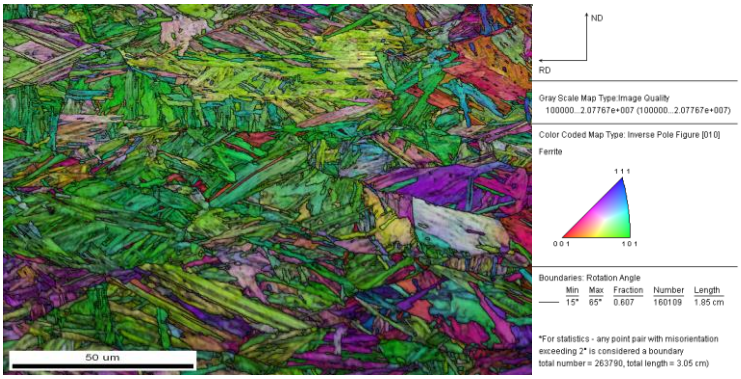

0.035Nb3.3Cr

Appendix 2: Transition curves in longitudinal (left) and transversal (right) direction of investigated steel.

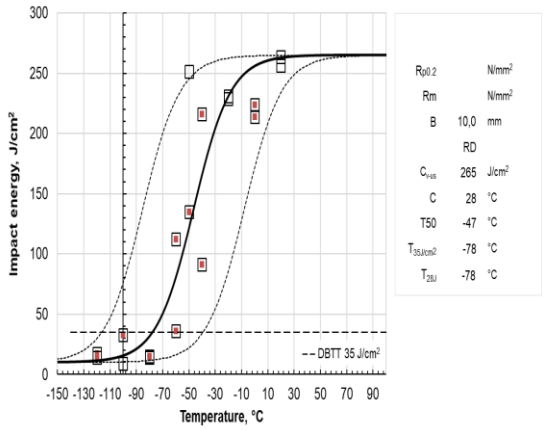

0.06Nb4Cr

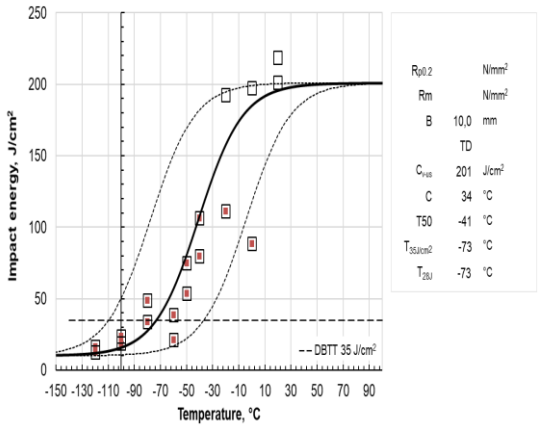

0.06Nb4Cr

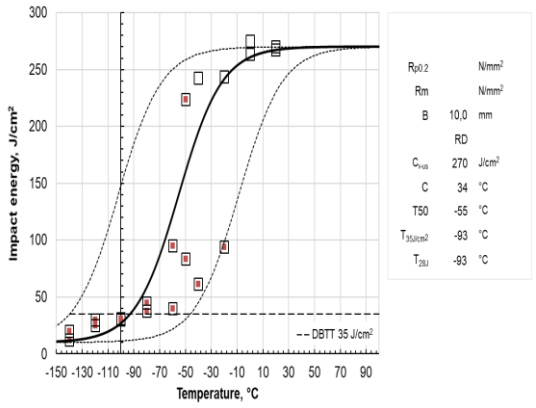

0.06Nb2.5Cr

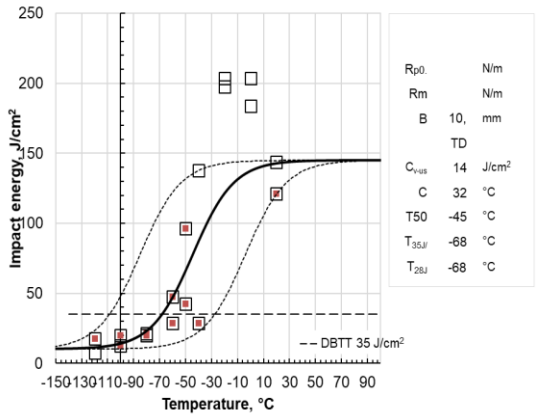

0.06Nb2.5Cr

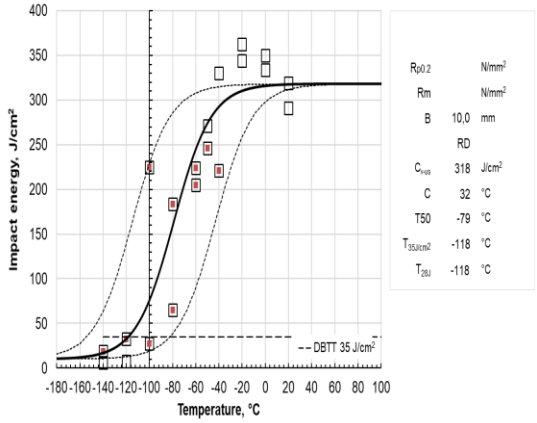

0.06Nb1Cr

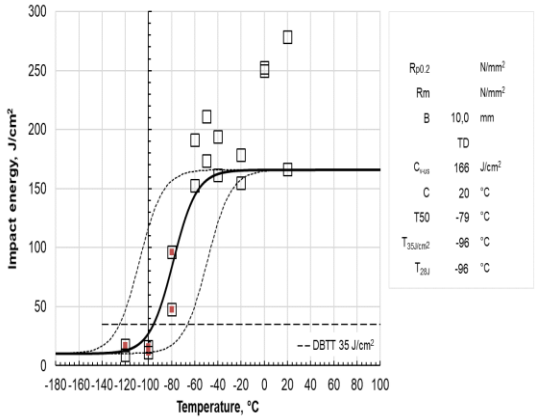

0.06Nb1Cr

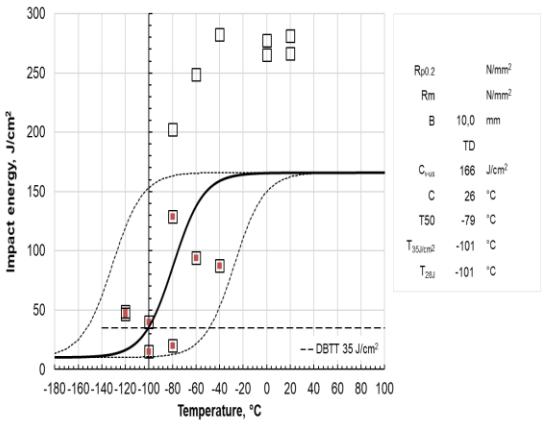

0Nb2.5Cr

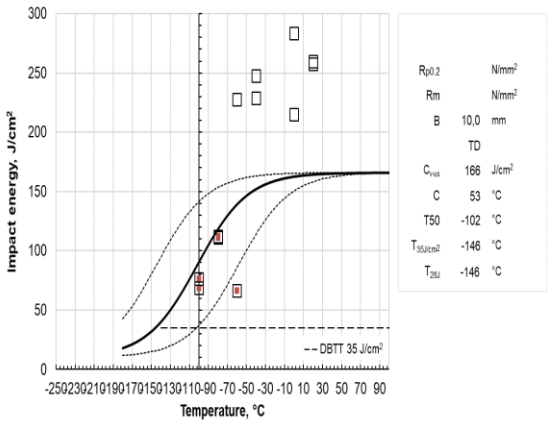

0Nb2.5Cr

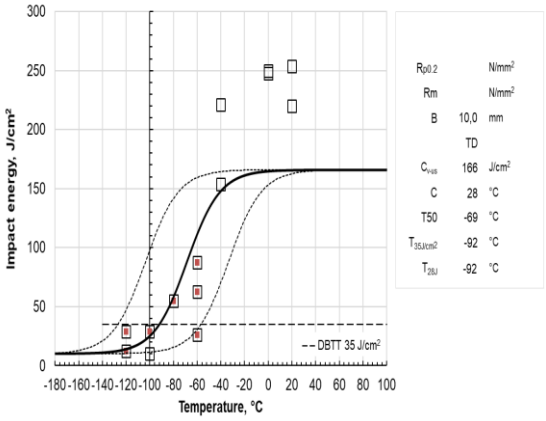

0Nb4Cr

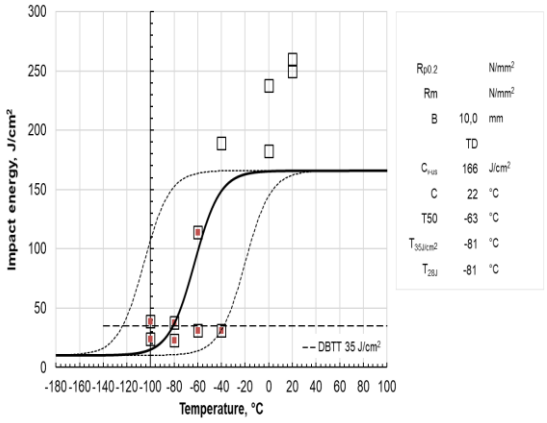

0Nb4Cr

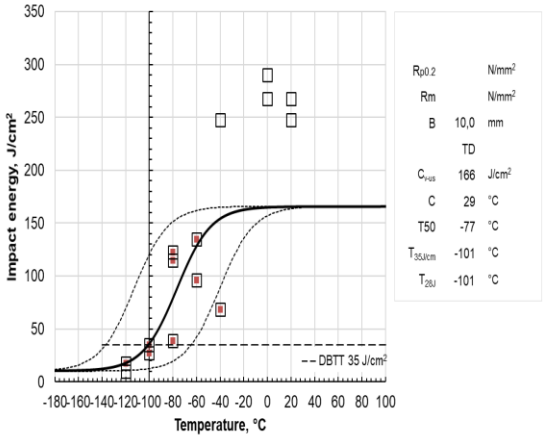

0.035Nb3.3Cr

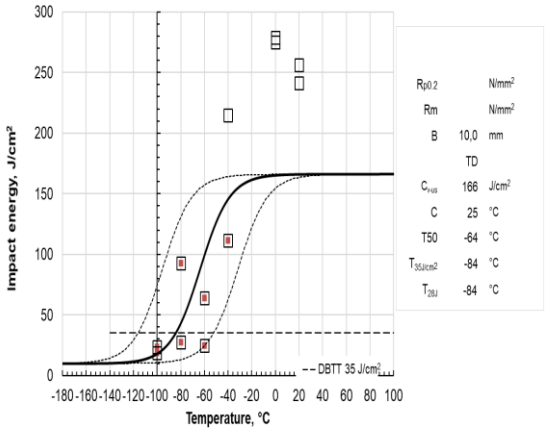

0.035Nb3.3Cr

Appendix 3: Regression analysis using Minitab

Regression Analysis: Rp0,2 versus Nb; Cr

Analysis of Variance

Source	DF	Adj SS	Adj MS	F-Value	P-Value
Regression	2	116334	58166,8	112,24	0,000
Nb	1	7381	7381,1	14,24	0,002
Cr	1	83788	83787,6	161,68	0,000
Error	15	7773	518,2		
Lack-of-Fit	3	6647	2215,8	23,61	0,000
Pure Error	12	1126	93,8		
Total	17	124107			

Model Summary

S	R-sq	R-sq(adj)	R-sq(pred)
22,7646	93,74%	92,90%	90,80%

Coefficients

Term	Coef	SE Coef	T-Value	P-Value	VIF
Constant	559,3	20,4	27,46	0,000	
Nb	-760	201	-3,77	0,002	1,10
Cr	69,14	5,44	12,72	0,000	1,10

Regression Equation

Rp0,2 = 559,3 - 760 Nb + 69,14 Cr

Regression Analysis: Rm versus Nb; Cr

Analysis of Variance

Source	DF	Adj SS	Adj MS	F-Value	P-Value
Regression	2	133479	66739,3	117,55	0,000
Nb	1	10394	10394,0	18,31	0,001
Cr	1	92715	92714,7	163,30	0,000
Error	15	8517	567,8		
Lack-of-Fit	3	7269	2423,1	23,31	0,000
Pure Error	12	1247	103,9		
Total	17	141995			

Model Summary

S	R-sq	R-sq(adj)	R-sq(pred)
23,8279	94,00%	93,20%	91,32%

Coefficients

Term	Coef	SE Coef	T-Value	P-Value	VIF
Constant	763,0	21,3	35,79	0,000	
Nb	-902	211	-4,28	0,001	1,10
Cr	72,73	5,69	12,78	0,000	1,10

Regression Equation

Rm = 763,0 - 902 Nb + 72,73 Cr

Regression Analysis: A % versus Cr

Analysis of Variance

Source	DF	Adj SS	Adj MS	F-Value	P-Value
Regression	1	44,101	44,1014	43,78	0,000
Cr	1	44,101	44,1014	43,78	0,000
Error	16	16,119	1,0074		
Lack-of-Fit	4	13,225	3,3063	13,71	0,000
Pure Error	12	2,893	0,2411		
Total	17	60,220			

Model Summary

S	R-sq	R-sq(adj)	R-sq(pred)
1,00370	73,23%	71,56%	65,99%

Coefficients

Term	Coef	SE Coef	T-Value	P-Value	VIF
Constant	17,907	0,702	25,51	0,000	
Cr	-1,514	0,229	-6,62	0,000	1,00

Regression Equation

A % = 17,907 - 1,514 Cr

Regression Analysis: Ag versus Cr

Analysis of Variance

Source	DF	Adj SS	Adj MS	F-Value	P-Value
Regression	1	17,3596	17,3596	47,23	0,000
Cr	1	17,3596	17,3596	47,23	0,000
Error	16	5,8804	0,3675		
Lack-of-Fit	4	5,1071	1,2768	19,81	0,000
Pure Error	12	0,7733	0,0644		
Total	17	23,2400			

Model Summary

S	R-sq	R-sq(adj)	R-sq(pred)
0,606238	74,70%	73,12%	67,08%

Coefficients

Term	Coef	SE Coef	T-Value	P-Value	VIF
Constant	6,577	0,424	15,51	0,000	
Cr	-0,950	0,138	-6,87	0,000	1,00

Regression Equation

Ag = 6,577 - 0,950 Cr

Regression Analysis: T28J lo versus Nb; Cr

Analysis of Variance

Source	DF	Adj SS	Adj MS	F-Value	P-Value
Regression	2	2223,54	1111,77	41,59	0,000
Nb	1	303,48	303,48	11,35	0,004
Cr	1	2210,82	2210,82	82,71	0,000
Error	15	400,96	26,73		
Lack-of-Fit	3	400,96	133,65	*	*
Pure Error	12	0,00	0,00		
Total	17	2624,50			

Model Summary

S	R-sq	R-sq(adj)	R-sq(pred)
5,17020	84,72%	82,69%	79,35%

Coefficients

Term	Coef	SE Coef	T-Value	P-Value	VIF
Constant	-135,74	4,63	-29,34	0,000	
Nb	154,0	45,7	3,37	0,004	1,10
Cr	11,23	1,24	9,09	0,000	1,10

Regression Equation

T28J lo = -135,74 + 154,0 Nb + 11,23 Cr

Regression Analysis: T28J tr versus Nb; Cr

Analysis of Variance

Source	DF	Adj SS	Adj MS	F-Value	P-Value
Regression	2	7607,4	3803,69	10,81	0,001
Nb	1	6237,2	6237,21	17,72	0,001
Cr	1	3466,4	3466,36	9,85	0,007
Error	15	5278,6	351,91		
Lack-of-Fit	3	5278,6	1759,54	*	*
Pure Error	12	0,0	0,00		
Total	17	12886,0			

Model Summary

S	R-sq	R-sq(adj)	R-sq(pred)
18,7592	59,04%	53,57%	38,85%

Coefficients

Term	Coef	SE Coef	T-Value	P-Value	VIF
Constant	-159,1	16,8	-9,48	0,000	
Nb	698	166	4,21	0,001	1,10
Cr	14,06	4,48	3,14	0,007	1,10

Regression Equation

T28J tr = -159,1 + 698 Nb + 14,06 Cr